Research Square

Preprints are preliminary reports that have not undergone peer review.
They should not be considered conclusive, used to inform clinical practice,
or referenced by the media as validated information.

In silico design of potent antioxidant compounds using 2D-QSAR Molecular docking ADMET prediction and Molecular dynamic simulation

Muhammad Baba Muhammad

etsufm247@gmail.com

Ahmadu Bello University

Adamu Uzairu

Ahmadu Bello University

Mohamed EL-fadili

Sidi Mohamed Ben Abdellah University

Stephen Eyije Abechi

Ahmadu Bello University

Muhammad Tukur Ibrahim

Ahmadu Bello University

Somdutt Mujwar

Sidi Mohamed Ben Abdellah University

Research Article

Keywords: ADMET, QSAR, Molecular docking, ROS, Antioxidants

Posted Date: July 2nd, 2026

DOI: https://doi.org/10.21203/rs.3.rs-9927797/v1

License: This work is licensed under a Creative Commons Attribution 4.0 International License.
Read Full License

Additional Declarations: No competing interests reported.

In silico design of potent antioxidant compounds using 2D-QSAR Molecular docking ADMET prediction and Molecular dynamic simulation

[1]Muhammad Baba Muhamad, Adamu Uzairu[2], Mohamed El fadili[2], Stephen Eyijeh Abechi[2], Muhammad Tukur Ibrahim[2], Somdutt Mujwar[2].

Email address of corresponding author: etsufm247@gmail.com

[1]*Faculty of Natural Sciences, Department of Chemical Sciences, Federal Polytechnic Bida, Niger State, Nigeria.*

[2]*Faculty of Physical sciences, Chemistry Department, Ahmadu Bello University, P.M.B. 1044 Zaria, Kaduna State, Nigeria.*

Keywords: ADMET; QSAR; Molecular docking; ROS; Antioxidants

Abstract

Background: Oxidative stress caused by free radicals plays a major role in the development of aging and several degenerative disorders, including cancer, cardiovascular diseases, diabetes, and Alzheimer's disease. Therefore, the discovery of potent antioxidant agents remains an important research focus. This study aimed to design new antioxidant compounds (benzoxazine derivatives) using a ligand-based approach involving QSAR analysis, molecular docking, molecular dynamic simulation, and ADMET prediction.

Methods: A QSAR model was developed using twenty-eight benzoxazine derivatives with the aid of Material Studio v8.0. Applicability domain and virtual screening were employed to identify a suitable template compound, which was subsequently modified to design new potent analogues. Molecular docking was performed against cytochrome c peroxidase (PDB ID: 2XO8) using Molegro Virtual Docker software. SwissADME and pkCSM servers were used to predict drug-likeness and pharmacokinetic properties.

Results: Among the four generated QSAR models, model four was selected as the best model based on its statistical parameters ($R^2_{ext} = 0.7449$, $R^2_{trn} = 0.7889$, $R^2_{adj} = 0.7361$, $Q^2_{LOO} = 0.6889$, and $cR^2p = 0.6015$). The designed compounds exhibited improved predicted antioxidant activities ($pIC_{50} = 8.002 - 8.532$), compared with the template and ascorbic acid ($pIC_{50} = 7.817$). Docking results revealed D5, D1, and D4 as having notable MolkDock scores of -135.37 kcal/mol, -134.38 kcal/mol, and -131.14 kcal/mol respectively. Furthermore, the molecular dynamic simulation and ADMET results revealed the stability of D1 and D2 design complexes, favorable drug-likeness, and good pharmacokinetic profiles.

Conclusions The designed benzoxazine derivatives may serve as promising antioxidant agents subject to further in vitro and in vivo experiments.

Introduction.

The high rise and spread of antimicrobial resistance in bacteria and fungi, attributed to inaccurate prescription and indiscriminate use of antibiotics, have dramatically increased health issues and have become one of the top leading causes of death worldwide [1]. According to the WHO, the mortality figures due to AMR will compete with other infectious diseases or exceed 50 million by 2050. Besides that, cellular death posed by bactericidal antibiotics induces damaging proteins, lipids and DNA through the production of reactive oxygen species (ROS) and as other free radicals [1, 2]. Reactive oxygen species (ROS) produced during normal metabolic processes in human cells are required for regular cell functions and neurological signal transmission [2]. However, excess production of these reactive oxygen species exposed the human body to various detrimental effects [3]. Consequently, these dangerous species can damage human cells by destroying cell membrane lipids and causing the cleavage of DNA [1]. Subsequently, the damage will eventually result in oxidative stress, which creates many risks in the human body and exposes it to various pathological conditions, such as atherosclerosis, cardiovascular diseases, cancers, and neurodegenerative ailments like Alzheimer's and pulmonary conditions [3].

Oxidative stress occurs when there is an imbalance between the production of free radicals and the ability of the body to counteract these reactive species via the application of endogenous and exogenous antioxidants [3, 4]. The imbalance can further cause inflammation, reduced muscle function, premature fatigue, and even cellular apoptosis [4]. To avert this threat, the body's endogenous antioxidant defense system, which includes cytochrome c peroxidase plays an essential role in maintaining damaged cells [4]. Cytochrome c is a multifunctional enzyme that plays a critical role in the mitochondrial electron transport chain [3]. Beyond its crucial function in the production of ATP, it also participates in the regulation of apoptosis. When severe oxidative stress occurs, the enzyme can be released from mitochondria into the cytosol, where it initiates programmed cell death. This process helps to eliminate severely damaged cells and maintain redox homeostasis [3]. These adaptive responses make cytochrome c peroxidase as attractive and rational target in the search for potent antioxidant agents [5].

Natural or synthetic antioxidants are compounds that are capable of interacting with free reactive oxygen species and inhibiting the oxidation process via termination of chain reactions before damaging the vital molecules [6]. During the last decade, heterocyclic compounds, which include

benzoxazines, benzodioxine, and its derivatives, have emerged as possible antioxidants [5]. Small molecules such as vitamin C, vitamin E, and vitamin A function as intracellular antioxidant systems by scavenging most reactive oxygen species that are produced in small amounts during normal physiological conditions [1]. Nevertheless, excess levels of ROS are required to be eliminated through the intake of highly potent antioxidant agents to discourage damage to the body [6]. Furthermore, natural products like curcumin, chalcones, quercetin, resveratrol, quinolines, etc. were also reported as antioxidants but were found to be associated with drawbacks such as poor solubility, low abundance, and severe toxicity [5]. These limitations suggest the urgent need to design and develop better therapeutic options that can improve treatment efficacy, mimic total drug resistance, support the standard drug (vitamin C, tocopherol), and eventually lead to the elimination of age-related disorders.

1,2-, 1,3-, and 1,4-benzoxazines are considered one of the major classes of organic compounds bestowed with a wide spectrum of biological activities [7]. Specifically, 1,4-benzoxazines represent a significant and privileged scaffold in drug discovery due to their potential pharmacological properties [7, 8]. They have been investigated to act as potential antioxidants, antidiabetics, antimicrobials, and anticancer agents, as well as act against neurodegenerative and cardiovascular disorders [7, 9]. This process occurs through mechanisms such as radical adduct formation, sequential proton loss, electron transfer, and hydrogen atom transfer. These reactions neutralize reactive radicals, preventing further cellular damage [10].

The rationale for this research study is that biological activities (antioxidant) of 1,4-benzoxazine derivatives have been reported, but there exists a paucity of comprehensive, detailed reports evaluating their therapeutic applications. Specifically, evaluations of the mathematical link that exists between 1,4-benzoxazine structures and their response activities, their binding mode interactions, drug-likeness, pharmacokinetic profiles, stability of newly designed ligand/protein complexes, and toxicity profiles are limited. Considering these factors, there is a need for advancing benzoxazine derivatives from experimental research to practical therapeutic agents. The concept of QSAR is crucial as it relates to the physiological functions of diverse compounds, coupled with even the yet-to-be synthesized ones. The docking study is essential as its paves the way for understanding the interactions between benzoxazine and the cytochrome c peroxidase enzyme; drug-likeness is also important for determining the potency of a given compound. The

molecular dynamic simulation helps reveal structural perturbations that influence the stability, binding thermodynamics, and pharmacokinetic feasibility of cytochrome c peroxidase inhibitors. This will aid in the rational design of novel antioxidant agents. Moreover, detailed pharmacokinetic profiling of newer derivatives, which are crucial for assessing the absorption, distribution, metabolism, and excretion, is insufficiently explored [9].

Computational approaches applied to identify new potent drugs were established to facilitate the drug discovery process, as they reduce time and cost and facilitate the assessment of properties of new improved drugs, such as their effectiveness and problems, before their synthesis [10]. In silico tools such as 2D-QSAR, molecular docking, molecular dynamics simulation, and ADMET (absorption, distribution, metabolism, excretion, and toxicity) predictions can be used to save time and reduce the cost of discovering drugs [11]. Therefore, the primary objective of this study was to unravel potent, exciting, and harmless antioxidants using a computer-aided drug technique. This investigation focused on addressing 2D-QSAR, molecular docking, structure-based design, drug-likeness, ADMET analysis, and molecular dynamic simulation of twenty-eight (28) benzoxazine derivatives. The QSAR study was performed to establish correlations between molecular descriptors and biological activity, guiding the rational design of improved drugs with better potencies of oxidative stress inhibitors. Molecular docking simulations were performed in order to gain insight into the nature of ligand-receptor interaction, and establish the strength of their interactions. Molecular dynamics simulations were also performed to validate the docking results and provide knowledge of their binding stability. In addition, drug-likeness and pharmacokinetic profiling were performed to evaluate the safety and efficacy of a drug in the body system. This study will not only unveil the structural properties of these compounds but will also examine their toxicity profiles, which could lead to enhanced drug design.

Table 1. Chemical structures of 1,4-benzoxazines derivatives

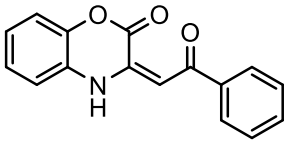
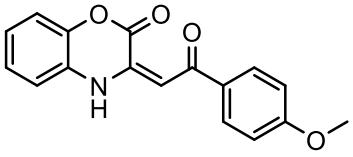
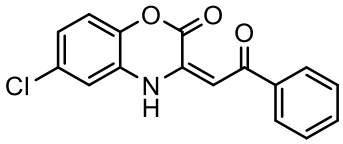
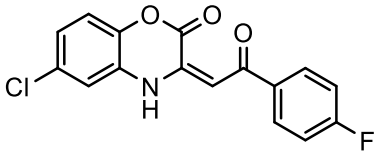
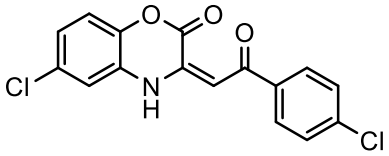
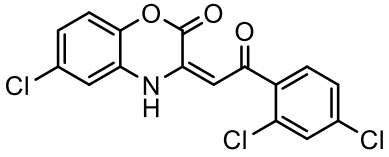
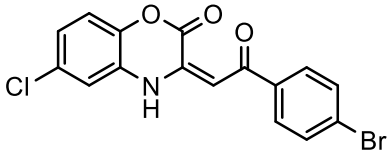
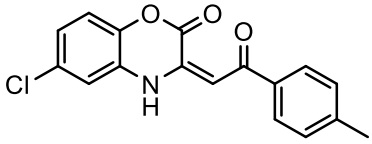
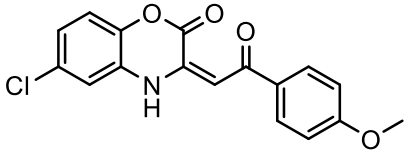
S/No	Compound	IC_{50} ($\mu g\ mL^{-1}$)	IC_{50} (μM)	pIC_{50}
1x		10.20	0.038	7.416
2y		6.89	0.023	7.633
3y		28.80	0.095	7.020
4y		45.20	0.142	6.847
5x		92.20	0.275	6.560
6y		56.60	0.153	6.814
7y		61.23	0.162	6.790
8y		44.83	0.142	6.845
9x		34.94	0.105	6.977

Table 1 continue

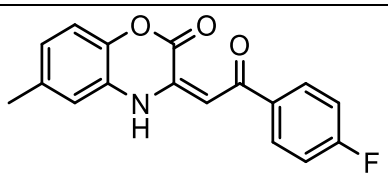
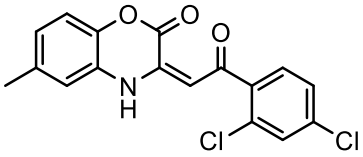
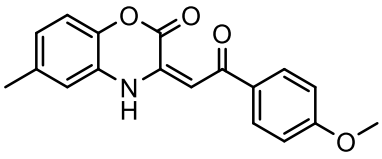
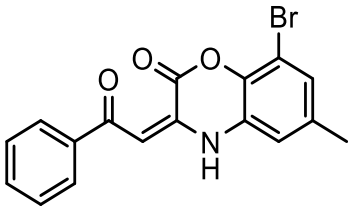
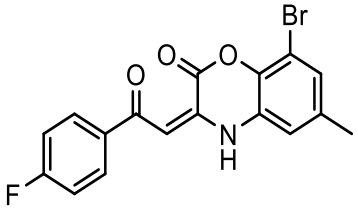
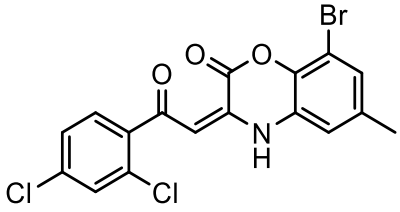
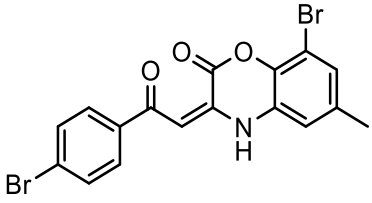
S/No	Compound	IC_{50} ($\mu g\ mL^{-1}$)	IC_{50} (μM)	pIC_{50}
10y		34.41	0.115	6.937
11y		43.58	0.124	6.903
12y		43.80	0.141	6.850
13x		24.38	0.067	7.168
14y		16.86	0.044	7.349
15y		22.48	0.052	7.278
16y		44.32	0.101	6.993

Table 1 continued

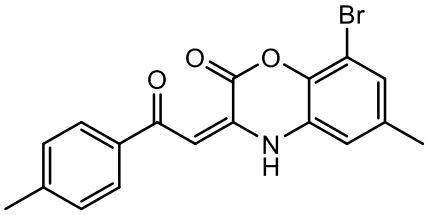
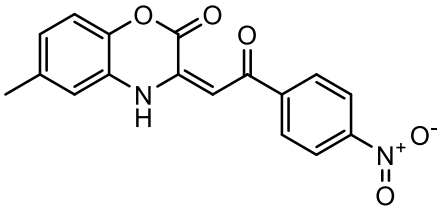
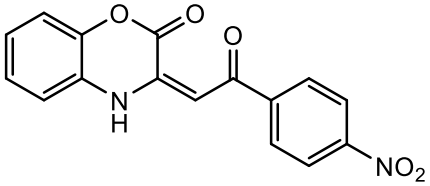
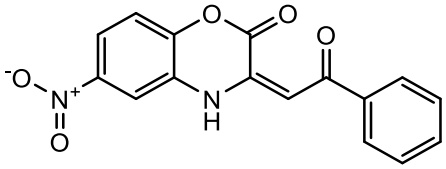
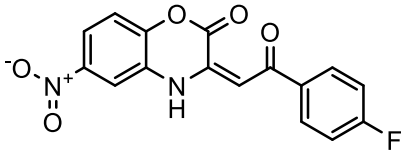
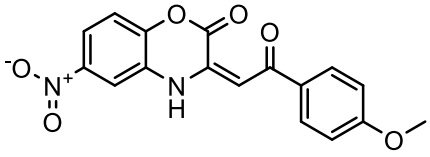
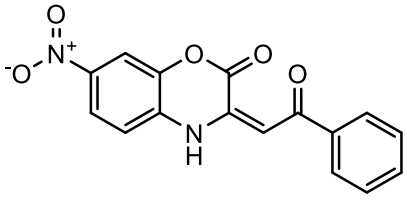
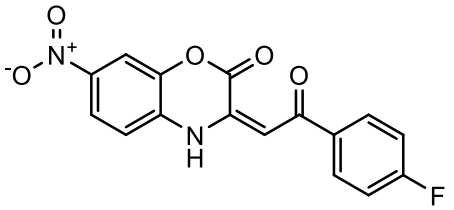
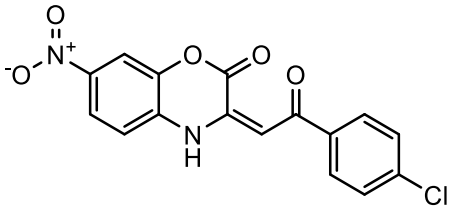
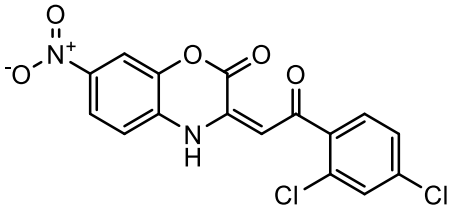
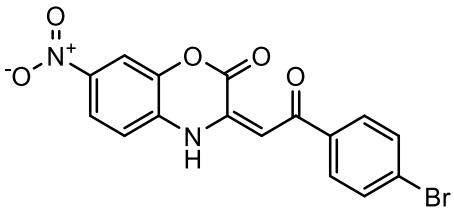
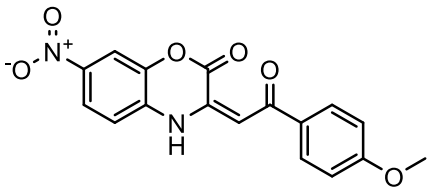
S/No	Compound	IC_{50} ($\mu g\ mL^{-1}$)	IC_{50} (μM)	pIC_{50}
17x		36.24	0.097	7.012
18y		12.23	0.037	7.424
19y		21.27	0.068	7.165
20y		4.74	0.015	7.817
21x		32.11	0.097	7.010
22y		43.58	0.127	6.893
23y		12.53	0.040	7.394

Table 1 continued

S/No	Compound	IC_{50} ($\mu g\ mL^{-1}$)	IC_{50} (μM)	pIC_{50}
24y		10.18	0.030	7.509
25x		19.76	0.057	7.242
26y		28.81	0.076	7.119
27y		28.37	0.072	7.138
28y		43.60	0.127	6.893

Y= Training set, X= Test set

2.0 Methods

2.1 Data set collection and structure appraisal

Twenty-eight (28) compounds of 1,4-benzoxazine derivatives as antioxidant agents were picked out from the work of [5]. The biological activities of these compounds were reported and evaluated

against the DPPH radical scavenging assay to determine their antioxidant activities. The activity values of the compounds were reported as IC_{50} (µg/mL), which were initially converted to IC_{50} (μM) and were finally transformed to pIC_{50} ($pIC_{50} = -\log (IC_{50} \times 10^{-6})$ to minimise skewness. The chemical structures of 1,4-benzoxazine derivatives with their biological activities, which span from 6.56 to 7.82, were selected for the 2D-QSAR modelling and molecular docking (Table 1). The 2D chemical structures of the compounds were drawn using ChemDraw software and subsequently converted to 3D format using Spartan 14.0 software [12]. Energy minimisation of the compounds was initially performed using molecular mechanics force fields (MMFF) within Spartan v14.0 software. This process aids in the molecular docking approach because it assists in identifying the most biologically active conformation of each compound while considering the lowest energy. To attain more better convincing conformations and equilibrium geometrics, each compound further underwent geometry optimisation via Density Functional Theory (DFT) with the B3LYP functional and 6–31G* basis set [3, 11].

2.2 Molecular descriptor generation, pre-treatment and selection

The PADEL-Descriptor software was used to generate molecular descriptors that are responsible for the antioxidant activities of the compounds after geometry optimisation. The computed descriptors were pretreated by excluding redundant, non-informative, and highly intercorrelated descriptors [11]. Subsequently, the resulting data set was divided into a training set (75%) and a test set (25%). The division of the data set was performed through the use of Kennard-Stone algorithm software to ensure even distribution [10, 12].

2.3 2D-QSAR model building and validations

The genetic function algorithm (GFA), combined with multi-linear regression (MLR) in the Material Studio v8.0 software, was used to build the model utilising the training set compounds. The GFA gives a result population of models rather than a single model [10]. A QSAR model is performed usually to establish a relationship that exists between the training set compounds (independent variables) and their biological activity (dependent variables) [13]. The training set compounds were utilised for internal validations, while the test set compounds were utilised for the external validation parameters [10, 15]. The model's validity and predictive strength were evaluated through several statistical metrics such as correlation coefficient (R^2 training). adjusted R^2, cross-validation coefficient (R^2 cv), correlation coefficient of the external test set (R^2ext) and

lack-of-fit (LOF) scores (Sagiru *et al.,* 2022). The equations that defined these parameters are identified in equations (1, 2, 3, 4 and 5), respectively.

$$R^2 = 1 - \frac{\sum(Y_{obs} - Y_{pred})^2}{\sum(Y_{obs} - Y_{mntrng})^2} \quad (1)$$

$$R^2_{adj} = 1 - (1 - R^2)\frac{n-1}{n-p-1} \quad (2)$$

$$R^2_{cv} = 1 - \frac{\sum(Y_{pred} - Y_{obs})^2}{\sum(Y_{obs} - Y_{mntrng})^2} \quad (3)$$

$$R^2_{test} = 1 - \frac{\sum(Y_{pred} - Y_{obs})^2}{\sum(Y_{obs} - Y_{mntrng})^2} \quad (4)$$

Where Y_{obs} is the value of the experimental activity, Y_{pred} is the value of the predicted activity, Y_{mntrng} is the average activity of either the experimental activity or the predicted activity, p is the number of explicative variables in the model, and n is the sample size [14, 15]. The Lack-of-Fit (LOF) from Friedman was used to measure the fitness and capability of the model. The revised formula for Friedman's lack of fit is shown by Eq. 5 below.

$$\text{Friedman LOF} = \frac{SSE}{M[1 - \lambda(\frac{C+DP}{M})]^2} \quad (5)$$

Where SSE is the sum of squares of error, M is the number of molecules in the training set, λ is the safety factor, which ensures that the denominator is not equal to zero. C is the number of terms in the model, D is the user-defined smoothing parameter, and P is the number of descriptors in the model [11].

2.4 Y-randomisation test

The Y-randomisation test is a statistical tool used to evaluate the efficiency of any developed 2D-QSAR model obtained by the MLR method [14]. It is also used to evaluate a model's robustness and to confirm that the developed model is not a chance correlation [16]. The test is usually performed by shuffling Y values (observed activities) while keeping the X values (molecular descriptors) constant. It's expected that the newly generated QSAR models should possess low Q^2 and R^2 values [10]. For the model to be robust, the coefficient of determination for the Y-scrambling test (cR^2p) value is anticipated to be greater than 0.5 [15]. The equation for calculating the (cR^2p) is given in (Eq. 6).

$$cR^2p = R \times [R^2 - R^2r] \quad (6)$$

Where cR^2p is the coefficient of determination for the Y-scrambling test, R is the coefficient of determination for Y-randomisation and Rr is the average 'R' for random models.

2.5 Applicability domain

The applicability domain is a theoretical region in chemical space, as described by the nature of the chemicals in the training set, model descriptors, and modelled responses [17]. A model is considered robust, significant, reliable, and not extrapolated only if the predictions for the chemicals fall within the applicability domain [13, 17]. The applicability domain assists in detecting structural and response outliers for a developed QSAR model. Therefore, it's of great importance to identify molecules that are not correctly predicted in terms of activities [14]. The leverage approach, which is one of the most frequently used methods to verify whether a new chemical will lie within the structural model domain, was used in this study. The leverage value effect of each compound is calculated using equation 7.

$$h_i = x_t^i\left(X^T X\right)^{-1} x_i\right) i \quad (7)$$

Where x_i is the vector descriptive quantity to be found, X is an n times (k-1) matrix of the k descriptors' values of the model for n compounds of independent variables, and the exponent T is the transpose of the matrix i, is a positive integer 1, 2, 3 ---- n [14].

The Williams plot is used to establish the applicability domain within a square area [14]. Compounds with high leverage values predictions ($h > h^*$) are considered to be unreliable and are excluded from the applicability [17]. The critical value has been calculated using (Eq. 8).

$$h^* = 3\ (k + 1/n) \quad (8)$$

Where n is the number of training set compounds, and 'k' is the number of descriptors used to build the model. Compounds within the cutoff value of ± 3 regions are not classified as outliers since points lying within this region cover 99% of the evenly distributed data [10].

2.6. Variance inflation factor

The variance inflation factor is an essential statistical tool used to measure the degree of inter-correlation between the descriptors in the generated model [15]. Computed VIF scores for molecular descriptors (VIF< 10) indicate that the molecular descriptors used in building the model

are not orthogonal to one another [11]. While computed VIF scores of less than 1 indicate that there is no intercorrelation among the descriptors. VIF scores greater than 10 indicate that the model is not valid [15]. The VIF is defined in Eq. (9).

$$VIF = \frac{1}{1-R^2} \quad (9)$$

Where VIF is the variance inflation factor and R^2 is the correlation coefficient of the chosen model.

2.7. Molecular docking studies

A molecular docking study was performed on the twenty-eight (28) 1,4-benzoxazine derivatives with human antioxidant enzyme. The docking studies was performed using Molegro Virtual Docker (MVD) software, as it gives a better, high accuracy level of predicting binding modes and more precise results compared to other docking software [18]. The crystal structure of the receptor (PDB: 2X08) used for the docking study was retrieved from the protein data bank (RCSB). The receptor is a CCP (cytochrome c peroxidase) which plays a major role in defending the body against oxidative stress by neutralising hydrogen peroxide ($HOO^{\cdot}$) through the use of cytochrome c as an electron donor [19]. The receptor was made up of one chain with 293 amino acids; in the receptor lies the complexed ligand ascorbate linked with GLYS 41, PRO 44, VAL 45, ASP 37, ARG 184, and HIS 181. Prior to docking, the accuracy and reliability of the protein model was evaluated using some analytical tools. The PROCHECK server was used to assess the Ramachandran plot of the receptor, which indicates that 89.2%, 10.8%, 0.0%, and 0.0% of residues lie under the most favoured, additional allowed, generously allowed, and disallowed regions, respectively (Fig. 7). Thus, suggesting that the protein exhibits high structural quality [20]. The ERRAT quality factor for this protein structure was 96.49%, which indicates that the receptor displayed good resolution [12]. The Verify3D score further showed that 97.61% of the amino acid residues were in favourable environments because the 3D-1D average atomic model score was greater than 0.1 (Fig. 7). This suggests that amino acid residues present in the protein are good for docking analysis.

2.8 Preparation and active site prediction of the receptor

The 3D crystal of cytochrome c peroxidase (PDB: 2X08) receptor with a resolution of 2.1 Å was transferred to Molegro Virtual Docker (MVD) v6.0. Before docking computation, the complexed ligand in the target receptor, water molecules, and heteroatoms were removed. Possible missing

atoms were repaired (rebuilt); polar hydrogens were also added. The surface area of the receptor was identified to determine the binding site of the ligands; a maximum of four (4) cavities were detected, in which the highest cavity was selected. The active site was defined as a sphere with coordinates X: -8.97, Y: -5.18, Z: 9.67 and a radius of 15 Å. A docking protocol of 1500 iterations and a population size of 50 were used. For the docking calculations, all prepared ligands, and the reference standard ascorbic acid, were docked. After completion of the docking procedure, the resulting protein ligand complexes were evaluated using the MolDock score and Rerank score. Furthermore, the binding interaction of the ligand-receptor complexes formed was visualised and examined with the aid of Discovery Studio v 6.1.0.15350.

2.9. Ligand-based drug design

In order to obtain more potent 1,4-benzoxazine derivatives with better activities, a ligand-based drug design approach was employed using the chosen QSAR model equation. Compound twenty (20), with the highest experimental activity (pIC_{50} = 7.817), low residual value (0.28), favourable applicability domain inclusion, better binding interaction with the target receptor, and adherence to Lipinski's rule of five and Verber rule. The derivatives of the lead compound were designed by adding functional groups such as hydroxyl ion, methyl, methoxy, hydrogen and ethoxy at the D, X and Y positions of Fig. 10. Addition of these substituents was based on the knowledge of the descriptor impact in the model.

2.10. Drug-likeness and pharmacokinetics computations

The physicochemical and pharmacokinetic properties of the 1,4-benzoxazine derivatives were evaluated to assess the oral-bioavailability problems and body reaction to the absorbed drug. These predictions are carried out to reduce the attrition rates of drug candidates [21]. The SwissADME web tool (Swiss Institute of Bioinformatics, Lausanne, Switzerland) was used to compute the drug-likeness of the compounds. The adsorption, distribution, metabolism, excretion, and toxicity of the best-docked compounds were calculated using the pkCSM server [11, 22].

2.11 Molecular dynamics simulation studies

Molecular dynamics (MD) simulations were carried out to determine the structural integrity, binding stability and interaction pattern of the complexed D1 and D5 in the active site of the receptor cytochrome c peroxidase. The MD simulations of the best two complexes were carried

out using Schrödinger's Desmond software [23]. Each complex was solvated in a cubic water box (TIP3P model) along the x, y, and z axes, with buffer zones of 12 Å via Desmond's system builder. The system was neutralised by introducing counterions and supplemented with physiological ionic strength calibrated to 0.15 M NaCl prior to simulation. The OPLS_2005 force field, which governed the atomic interactions within each complex, was applied to describe all atomic interactions [24]. Following energy minimisation over 10,000 steepest descent step iterations, the systems were equilibrated at two stages: Equilibration at 310 K using a Nose–Hoover thermostat for 500 ps under the NVT ensemble, and Equilibration at 1 atm pressure under the NPT ensemble by 1 ns using a Martyna–Tobias–Klein barostat. In addition, production runs were carried out for 100 ns, with simulation snapshots recorded every 100 ps. Protein-ligand flexibility and stability were analysed through RMSD, RMSF, radius of gyration (Rg), and hydrogen bonding using the Simulation Interaction Diagram tool in Schrödinger's Desmond software [22, 24].

3.0 Results and Discussion

3.1. 2D QSAR modelling and validation results.

It's an established protocol in the field of chemistry, that the behavior of a molecule is a function of its molecular structure [21]. A reliable and robust predictive 2D-QSAR model was successfully generated to establish the relationship between molecular structure and response activity (pIC_{50}) against oxidative stress diseases. Out of the four QSAR models generated, model three (3) eq. (10) was selected as the best model based on the fact that it exhibited strong model fitting and satisfied the conditions set for QSAR validation metrics in Table 2. The Friedman's lack-of-fit (LOF) value of 0.1060 indicates a low degree of overfitting, indicating that the model maintains a sync correlation between complexity and predictive accuracy. The internal R^2 value of 0.7889 is an indicator that the selected model clarified an excessive proportion of the independent variable is sufficiently powerful for a QSAR model. The R^2 value suggests that 78.89% of the variance lies in the response activity defined by the model [10]. The adjusted R^2 value of 0.7361 further affirmed the model's dependability by accounting for the number of descriptors employed, ensuring that the model's predictive capability is not filled by irrelevant variables. The cross-validated coefficient (Q^2) of 0.6889, examined through internal validation, showcases strong internal consistency and predictive power within the training set compounds. Additionally, to further examine the robustness of the selected model, it was validated externally, and the external validation correlation

coefficient (R^2_{ext}) was found to be 0.7449. This value surpassed the minimum recommended value of ≥ 0.6 for an acceptable model [21]. The R-squared predicted value suggests that the model possesses an excellent fit for replicating antioxidant properties. The RMSE values for both the training set and test compound were also observed to be within the recommendable threshold. Therefore, we can confidently conclude that the selected model will predict the antioxidant activity of the 1,4-benzoxazine derivatives accurately. The model's efficiency and resilience meet the traditional evaluation criterion. Model four has passed all the recommended criteria for accepting the developed QSAR model. Equations 9, 10, 11, and 12 present the four developed QSAR models, each with their four (4) descriptors.

QSAR model 1

pIC_{50} = 0.1470*(ALogp2) -2.8153*(AATS1p) +2.6016*(MATS3m) -5.6325*(SpMin6_Bhv) +18.766 (10)

QSAR model 2

pIC_{50} = 0.1311*(ALogp2) -2.7257*(AATS1p) -2.8128*(GATS3m) -6.7276*(SpMin6_Bhv) +22.2224 (11)

QSAR model 3

pIC_{50} = 3.5332*(GATS2m) -3.4784*(GATS3m) -7.5355*(SpMin6_Bhv) + 0.8909*(IC2) +12.2882 (12)

QSAR model 4

pIC_{50} = 3.8808*(GATS2m) -3.6510*(GATS3m) -7.0938*(SpMin6_Bhv) +6.0646*(BIC2) +10.8795 (13)

Table 2. Statistical validation of the 2D-QSAR models.

Internal validation	Threshold	Model 1	Model 2	Model 3	Model 4
Lack of fit (LOF)	Closer-zero	0.1049	0.1061	0.1060	0.1065
R^2_{train}	R^2 train > 0.6	0.7813	0.7893	0.7889	0.7883
Adjusted R^2	R^2 adj > 0.6	0.7392	0.7366	0.7361	0.7354
$R^2 - R^2_{adj}$	≤ 0.3	0.0421	0.0527	0.0628	0.0529
R^2_{ext}	R^2 pred > 0.5	0.3792	0.5010	0.7449	0.6336
Cross Validated Squared (Q^2)	Q^2 > 0.6	0.6524	0.6515	0.6889	0.6328
Y-randomization (cR^2 p)	cR^2 p ≥0.5	0.6113	0.6289	0.6015	0.5429
Critical SOR F-value (95%)	-	3.0558	3.0558	3.0558	3.0558
Significant Regression	Yes	Yes	Yes	Yes	Yes
$RMSE_{test}$	Low	0.2034	0.1823	0.1303	0.1562
$RMSE_{test}$	Low	0.1330	0.1337	0.1338	0.1340

(Abdullahi *et al.,* 2023; Philip *et al.,* 2025)

Model 4 contains various computed molecular descriptors, such as GATS2m, GATS3m, SpMin6_Bhv and IC2, which influence antioxidant activity. It was observed that the descriptors

SpMin6_Bhv and IC2 were positively correlating and contributing towards antioxidant activity, while the descriptors GATS2m and GATS3m were negatively contributing to the antioxidant activity. The positive coefficients for the descriptors SpMin6_Bhv (spectral minimum eigenvalue from burden matrix) and IC2 (information content – order 2) indicate that they will greatly favour the biological activity. This suggests that the biological activity of 1,4-benzoxazine derivatives can be improved by incorporating substituents that modulate lipophilicity, polarisability and structural complexity. Additionally, the molecular descriptors GATS2m and GATS3m, which represent Geary autocorrelation at lags 2 and 3 weighted by mass, indicate that they will negatively affect the biological activity of the compounds because of their negative coefficients. Conversely, the negative coefficients of Geary autocorrelation descriptors will hinder the activities of 1,4-benzoxazine derivatives. Table 3 represents a list of the descriptors, descriptions, and their classes.

Table 3. list of descriptors of model 3

S/No	Descriptor code	Description	Class
1	GATS2m	Geary autocorrelation -lag 2/weighted by mass	2D
2	GATS3m	Geary autocorrelation -lag 3/weighted by mass	2D
3	SpMin6_Bhv	Smallest absolute eigenvalue of Burden modified matrix-n 6/ weighted by relative van der Waals volumes	2D
4	IC2	Information content index (neighborhood symmetry of 2-order)	2D

The Y-randomisation test was ascertained through random shuffling of the biological activity while keeping the model descriptors of the training set constant. This resulted in the generation of random models [12]. The generated random models were accompanied by low R^2 and Q^2 values, which indicates that the developed model was robust, reliable, and not obtained by chance correlation [21, 22]. The coefficient value obtained for the Y-randomisation test (cR_P^2) of the best model was computed as 0.6015, which was within the minimum recommendable value for accepting a QSAR model (Table 4).

Table 4. Y-randomisation test of model 3 descriptors.

Model	R	R^2	Q^2
Original	0.777653	0.604745	0.431803
Random 1	0.410895	0.168834	-0.27965
Random 2	0.383044	0.146722	-0.33944
Random 3	0.26294	0.069138	-0.52402
Random 4	0.515096	0.265324	-0.12962
Random 5	0.438764	0.192514	-0.25347
Random 6	0.466703	0.217812	-0.01241
Random 7	0.201573	0.040632	-0.46169
Random 8	0.341257	0.116456	-0.4148
Random 9	0.16611	0.027592	-0.60557
Random 10	0.400927	0.160742	-0.3475
Random Models Parameters			
Average R	0.398731		
Average R^2	0.170577		
Average Q^2	-0.43682		
cR_P^2	0.601557		

The variance inflation factor, which is used to evaluate the intercorrelation between the descriptors of a developed model, was determined [21]. The variance influential factor was calculated using equation 13. Multiple linear regression in Microsoft Excel Office 16 was the statistical tool employed to calculate the VIF values of the selected model.

$$VIF = {}^{1}/_{1 - R^2} \quad (14)$$

Where VIF is the variance inflation factor and R^2 is the correlation coefficient of the chosen model.

The mean effect is an important statistical parameter used to evaluate the relative importance and direction of each descriptor in a generated QSAR [12]. A positive ME value suggests that increasing the value of the descriptor generally leads to improved biological activity. Conversely, a negative ME value suggests that higher values of the descriptor are typically associated with reduced activity. The mean effect values were calculated using equation (15).

$$ME_i = b_i \times \sum xi / \sum (b_j \times \sum xi) \quad (15)$$

Where 'bi' is the regression coefficient of the descriptor, i, x_i is the value of the descriptor for all compounds, and j represent all the descriptors in the model.

The Pearson correlation was calculated using the correlation statistical tool, Microsoft Excel Office 16. The correlation between the descriptors of the best model (3) is presented in Table 5. The VIF computation results revealed that the descriptors' VIF values fall within the recommended limit (< 5). This suggests absence of significant collinearity among the model descriptors. Hence, the descriptors were statistically independent and reliable. The mean effect scores of the four descriptors indicate that GATS3m and SpMin6_Bhv, with the mean effect scores of 0.6471 and 1.4763 indicate that these two descriptors contribute positively to the IC_{50} activity. Conversely, the descriptors GATS2m and IC2 contribute negatively to the IC_{50} activity. The descriptor SpMin6_Bhv has the highest positive contribution to the IC_{50} activity. Therefore, an increase in this descriptor value will enhance the IC_{50} activity. GATS3m also showed a positive contribution to IC_{50} activity, but to a minor extent. IC2 showed the strongest negative contribution, while GAT3m showed the least negative contribution. Therefore, an increase in this descriptor's values will exert low influence on the IC_{50} activity.

Table 5. The Pearson's correlation, VIF, and ME values model four

Descriptors	GATS2m	GATS3m	SpMin6_Bhv	IC2	VIF	ME
GATS2m	1				1.9075	-0.4232
GATS3m	-0.11028	1			1.1987	0.6471
SpMin6_Bhv	-0.22047	-0.0718	1		1.4913	1.4763
IC2	-0.66671	0.285497	0.498487	1	2.7546	-0.7004

Figures 1A and 1B represent the plot of experimental against predicted activity of both the training set and test set, which forecasts excellent reliability for the activity prediction of the model [25]. The predicted R^2 of 0.7889 obtained from the extrapolated graph (Fig. 1B) indicates strong correlation, suggesting that the model captures a good proportion of the variance in the experimental data [12]. Moreover, it can be inferred from the plot that there is a uniform distribution of data points with the line passing through the zero point of the graph. Additionally, the residual plot (Fig. 1D) indicates that the majority of residuals were tightly packed together around zero and display a random distribution without any observable pattern. This behavior affirms the absence of systematic errors and provides clear support that the model's predictions are in good agreement with the experimental results.

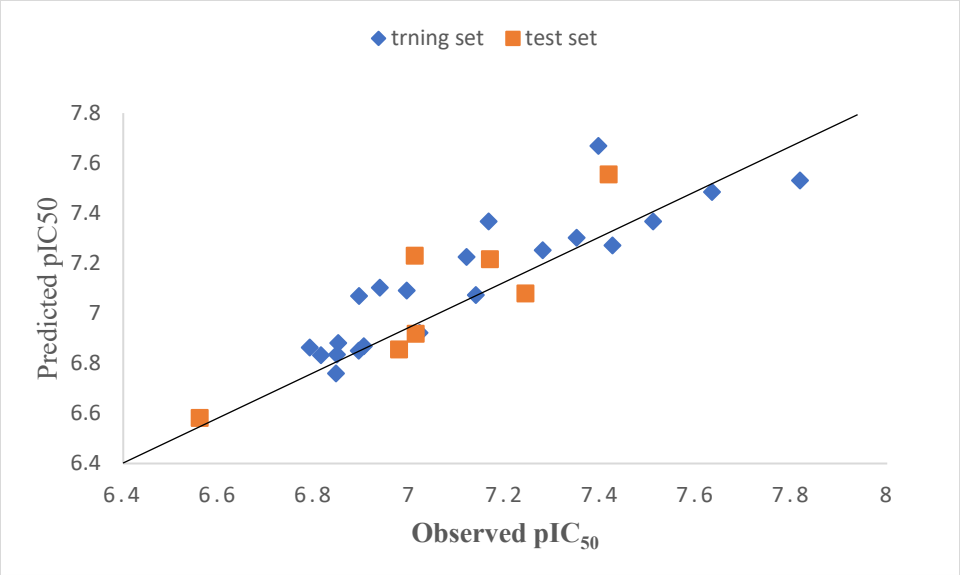


Fig 1A: Plot of experimental activity against predicted activity of training and test set



Fig 1B: Plot of experimental activity against predicted activity of training and test set

The applicability domain (AD) of the developed QSAR model was further defined by using the Williams plot (Fig. 1C). This graph was obtained through the plot of standardised residuals against leverage values. The plot, recommended by Gramatica and co-workers for routine AD assessment,

simultaneously helps detect structural influencers compounds whose leverage (h) exceeds the warning threshold and response outlier points with residuals beyond ±3 [12, 24]. The plot reveals that vast majority of compounds (90%), including both training and test sets, fall within the applicability domain, defined by the warning leverage (h^* = 0.72) and within ± 3 standard residuals. Compounds that fall within this boundary are considered structurally potent relative to the calibration set and can sway the regression coefficients. Notably, three compounds of the test set in the data set, namely (1, 5 and 9) exceed the warning leverage, suggesting that they are structurally influential. However, their standardised residuals are within the acceptable range (±3), which shows that they may influence the model but they do not qualify as response outliers [22].

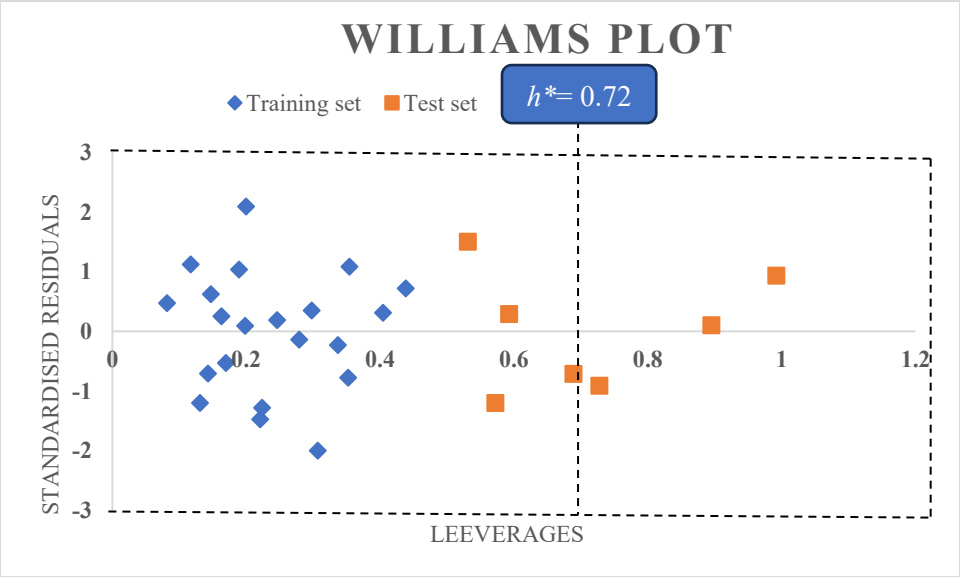


Fig 1C: Scatter plot of standardized residuals against Leverages of training set and test set

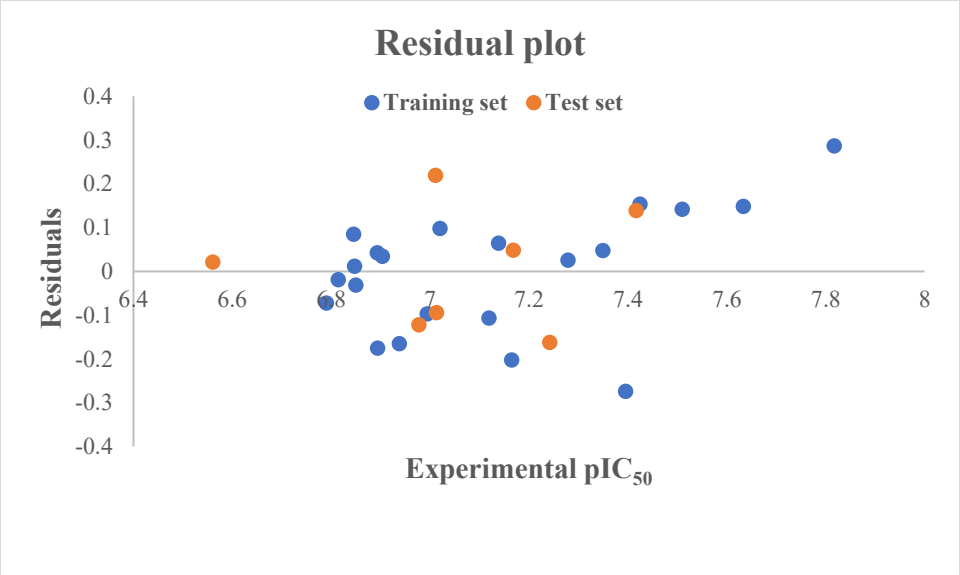


Fig 1D: Graphical plot of residuals against Experimental pIC_{50}

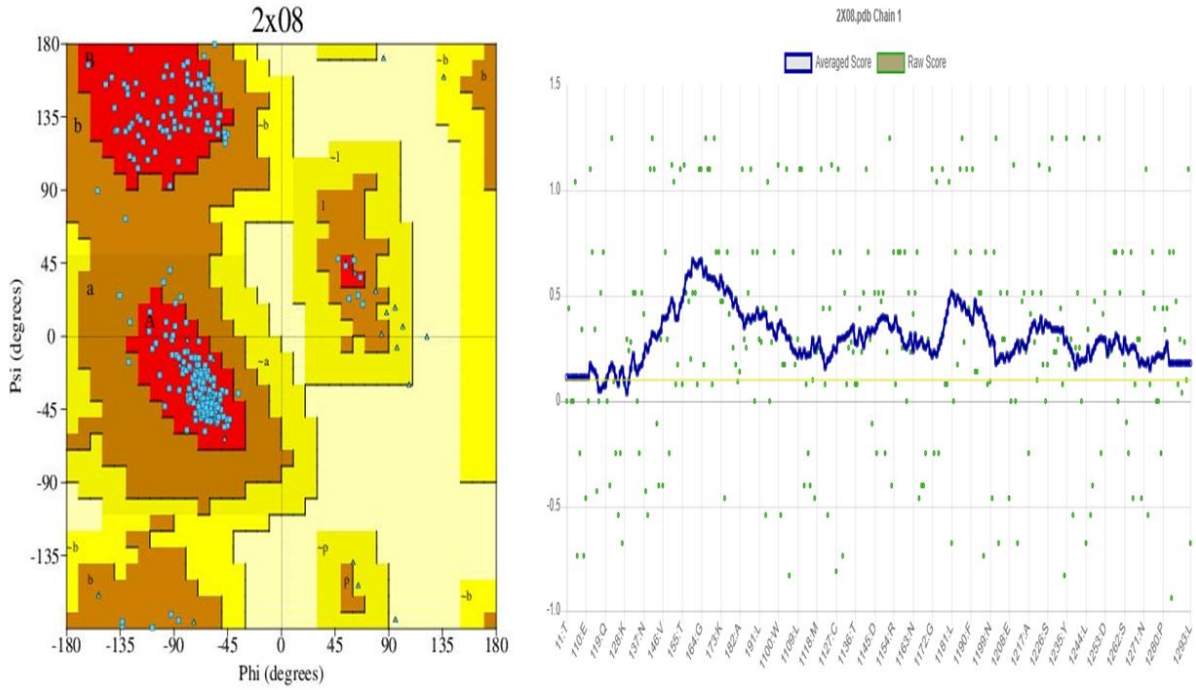


Fig 2: Validation and quality assessment of the receptor (2X08) by using (a) Ramachandran plot using PDBsum tool (b) Verify 3D plot using Procheck tool.

3.2. Molecular docking results of benzoxazine derivatives

Molecular docking is a widely acknowledged computational method used for probing the binding affinities and interactions between a ligand and a target protein [26]. In this study twenty-eight

(28) 1,4-benzoxazines derivatives were docked with cytochrome c peroxidase (PDB ID: 2XO8). Cytochrome c peroxidase is a multifunctional protein that plays a crucial role in the mitochondrial electron transport chain [27]. Beyond its vital function the production of ATP, cytochrome c also helps in the regulation of apoptosis. Under severe oxidative damage, it can be released from mitochondria into the cytosol, where it triggers programmed cell death, a process essential for removing severely damaged cells and maintaining tissue homeostasis [27]. The docking scores were examined using MolDock and the Rerank scoring function, with ascorbic acid use as the reference drug. The docking results of the 28 benzoxazine derivatives (Table 6) revealed that all the compounds bind favourably to the active sites of cytochrome c with binding energy values ranging from -116.88 kcal/mol to 151.56 kcal/mol. Notably, compounds 15, 22, 26, and 28 exhibit better binding scores compared to the reference compound (ascorbic acid), where the docking score observed was -82.772 kcal/mol (Table 6).

Examination of the mechanism of interaction of the compounds with the receptor revealed that compound 22, with the highest binding score of -151.56 kcal/mol, binds to the receptor via the formation of two carbon-hydrogen bond interactions with HIS 181 and ARG 48; a pi-sigma bond with ARG 48; a pi-sulphur bond with MET 172; four pi-pi stacked bonds with TRP 51; two amide-pi stacked bonds with LEU 171 and ALA 174; and five pi-alkyl interactions with 2TRP 51, PHE 158, HIS 181, and PHE 266 (Fig. 3). Compound 28, with the second-best score of -147.706 kcal/mol (Fig. 4), interacted with the cytochrome c peroxidase receptor via a single hydrogen bond with the amino residue ARG 48; two carbon hydrogen bonds with the amino residues HIS 181 and ARG 48; three pi-pi stacks with the amino residue TRP 51; an alkyl interaction with VAL 45; and eight pi-alkyl interactions with the amino residues PRO 44, VAL 47, HIS 181, 2ALA 174, and 2ARG 48. Compound 26, with the third best score of -146.649 kcal/mol, interacted with the cytochrome c peroxidase receptor, forming one hydrogen bond with the amino residue LYS 179; one carbon hydrogen bond with the amino residue GLYS 178; one pi-sulphur with the amino residue MET 172; two pi-pi stacks with the amino residue TRP 51; three amide-pi stacks with the amino residues VAL 47 and 2LEU 171; two alkyl interactions with LEU 171 and MET 172; and lastly, formed five pi-alkyl interactions with the amino residues PHE 158, 2ARG 48, PRO 44, and ALA 174 (Fig. 5). Compound 15, with the least-best score of -146.01 kcal/mol, interacted with the cytochrome c peroxidase receptor, forming two carbon-hydrogen bonds via the amino residues ARG 48 and HIS 171; one pi-sulphur with the amino residue MET 172; four pi-pi stacks with the

amino residue TRP 51; two amide-pi stacks with the amino residues LEU 171 and ALA 174; and four alkyl interactions with the amino residues MET 172, LEU 269 2LEU 171; and ten pi-alkyl interactions with the amino residues 2TRP 51, PHE 158, HIS 181, PHE 266, 2ARG 48, 2ALA 174, and LEU 171 (Fig. 6).

Conversely, ascorbic acid interacted with the cytochrome c peroxidase receptor, establishing five hydrogen bonds via the amino residues ARG 48, 2HIS 175, PRO 44, and LEU 177. It's evident from the 2D and 3D dimensional views of compounds 22, 26, 28, and 15 that they established more diversity of interactions with the receptor than the control compound (Fig. 7). Hence, the in silico studies suggest that compounds 22, 26, 28, and 15 possess promising potential as oxidative stress inhibitors.

Table: 6 Docking scores of 1,4-benzoxazine derivatives and hydrogen bond distance

S/No	MolDock sore	Rerank score	HBond distance
1	-116.88	-105.941	-7.96
2	-132.782	-112.709	-1.95
3	-123.86	-109.373	-2.5
4	-130.909	-114.018	-2.5
5	-130.18	-112.261	-2.49
6	-140.376	-118.504	-2.5
7	-131.591	-112.576	-2.5
8	-131.968	-115.501	-2.5
9	-140.222	-119.474	-4.71
10	-131.618	-115.988	-2.5
11	-142.219	-120.542	-2.5
12	-138.873	-119.708	-4.71
13	-129.542	-108.079	-2.5
14	-137.89	-119.954	-2.5
15	-146.01	-123.74	-2.5
16	-137.015	-118.193	-2.5
17	-135.93	-118.642	-2.5
18	-144.71	-128.54	-9.42
19	-129.395	-116.786	-6.27
20	-128.008	-111.355	-2.5
21	-142.332	-126.799	-2.5
22	-151.56	-132.955	-4.78
23	-134.456	-117.851	-2.80
24	-140.954	-116.723	-2.75
25	-142.052	-116.056	-2.97
26	-146.649	-127.004	-1.72
27	-139.913	-117.631	-2.87
28	-147.706	-132.433	-1.64
Vitamin C	-83.445	-73.30	-10.33

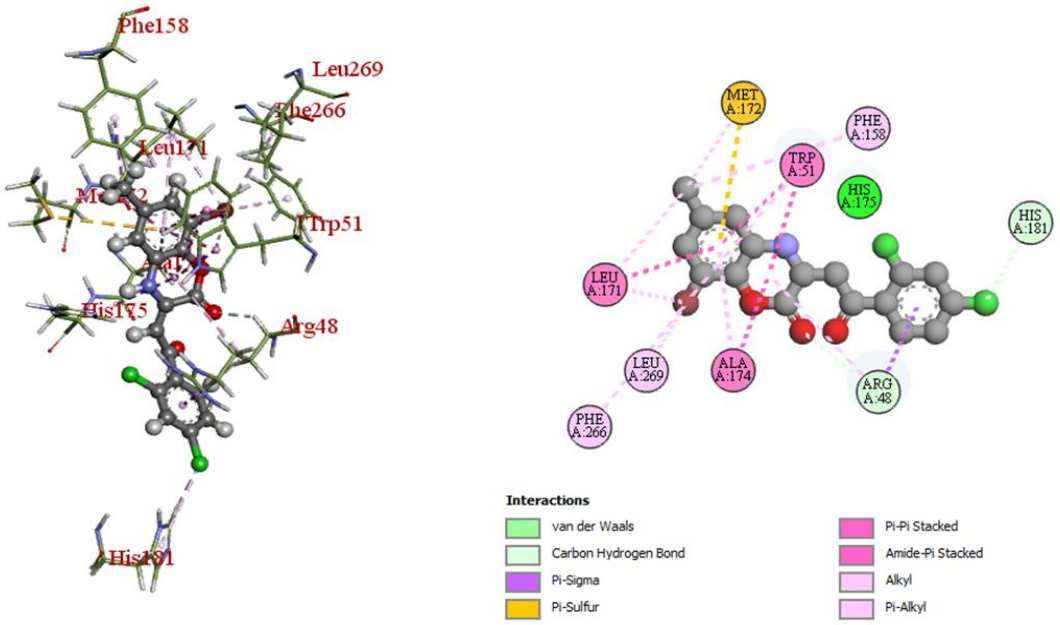


Fig. 3: 3D and 2D docking output view of compound 22 with the receptor (2XO8)

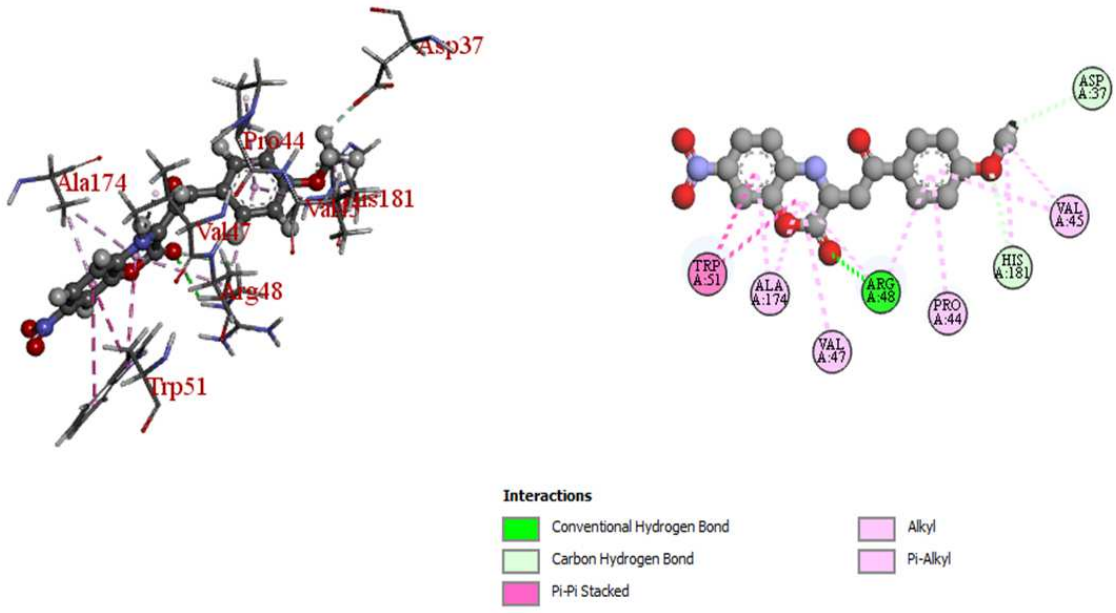


Fig. 4: 3D and 2D docking output view of compound 28 with the receptor (2XO8)

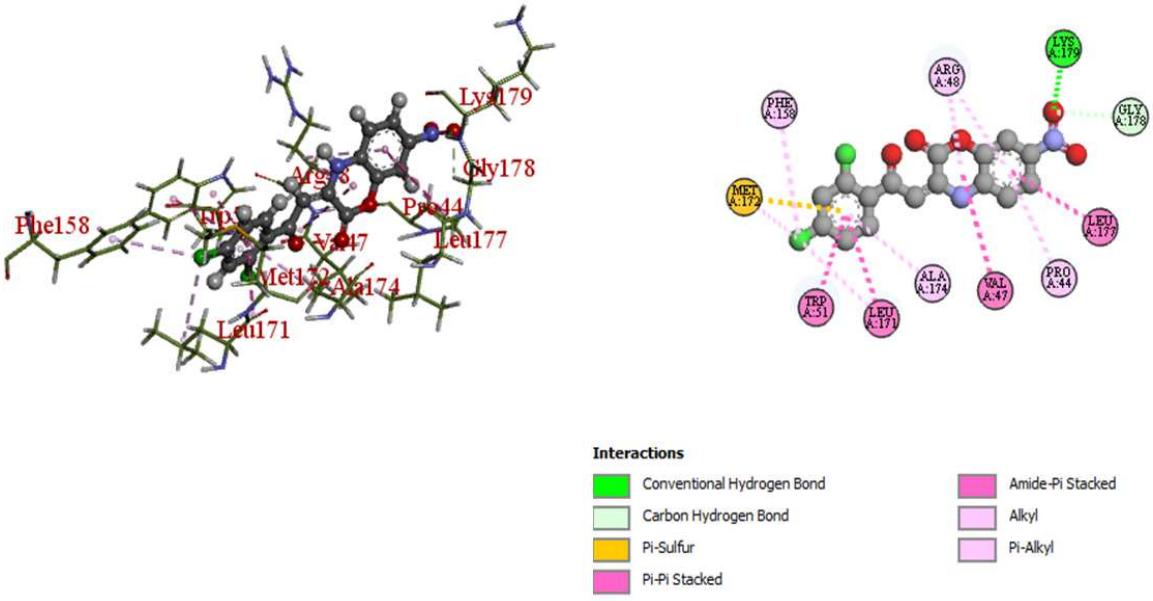


Fig. 5: 3D and 2D docking output view of compound 26 with the receptor (2XO8)

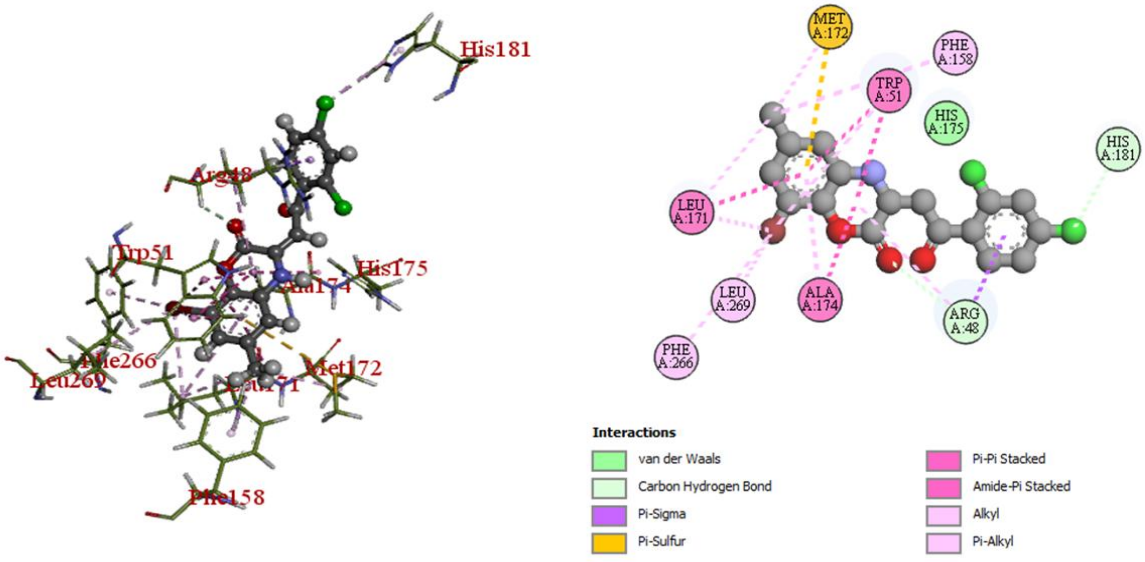


Fig. 6: 3D and 2D docking output view of compound 15 with the receptor (2XO8)

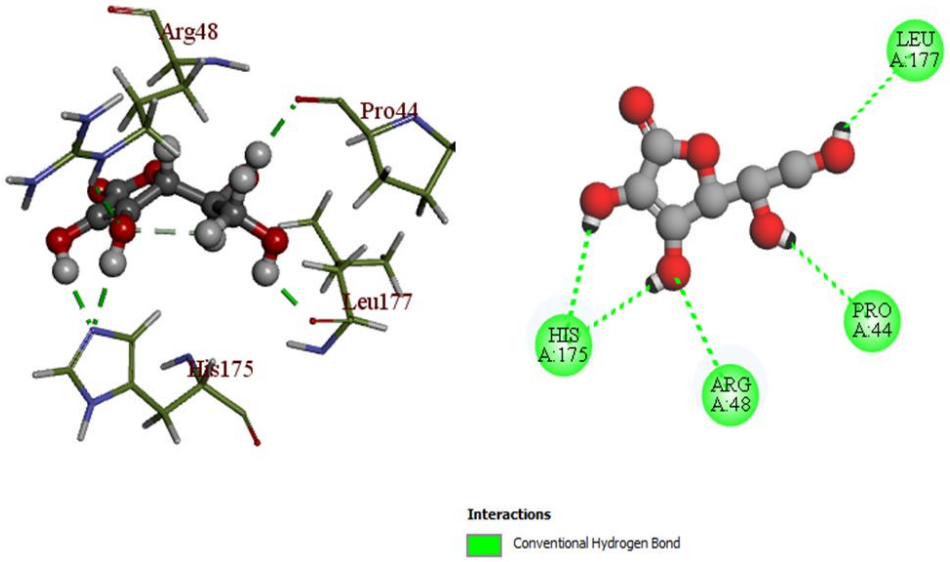


Fig. 7: 3D and 2D docking output view of vitamin c with the receptor (2XO8)

3.3 Ligand drug design results

An in silico ligand drug design was used to design new novel benzoxazine compounds with a pIC_{50} against oxidative stress diseases based on the chosen QSAR model. Compound twenty-one (20) was selected as the design template due to its notable experimental activity among the derivatives. The structure of compound 21 (Figs. 10 and 11) serves as a rational modification aimed at the introduction of substituents that enhance polarisability, and structural complexity that contribute to biological potency. Five functional groups were added onto the benzene and oxazine rings of the chosen benzoxazine scaffold at D, X and Y positions (Fig. 10). The functional groups added were methoxy (CH_3O), hydroxyl (OH), ethoxy (C_2H_5O), ethyl (C_2H_5) Chlorate (ClO^-) and aldehyde group (CHO). These substituents were added based on the positive contribution of GATS2m and IC2 descriptors in the QSAR model equation, which suggested that the addition of these substituents will enhance short-range mass distribution and moderate structural symmetry which favours antioxidant activity [1]. The reason for the addition of these substituents was based on in vitro antioxidant activity studies by Majed *et al.,* which showed that substituents such as CH_3O, CHO, and C_2H_5O containing oxygen atoms, and a small number of carbon atoms increase biological activity. Furthermore, these oxygen atoms enhanced the solubility degree of the drug in

aqueous media via the formation of excessive hydrogen bonds, which improves the candidate's in vitro antioxidant properties. Conversely, the strong negative contribution of SpMin6_Bhv suggested that excessive steric bulk adversely affects response activity. Hence, structural modifications were projected toward compact benzoxazine derivatives bearing small electron-donating substituents while avoiding bulky groups, branching chains, and side chain extensions [28]. Five (5) new compounds with superior biological activities, which span from pIC_{50} = 8.00 to 8.53, were designed. The new compounds were found to significantly possess better biological activities than the chosen template, which has pIC_{50} a 7.817. The chemical structures of the designed compounds are shown in Table 7.

3.4 Interpretation of molecular docking result of the designed compounds

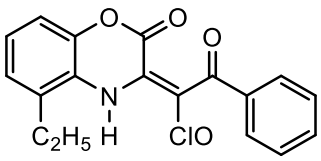
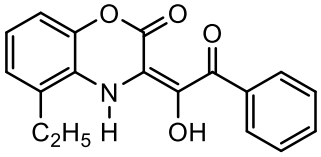
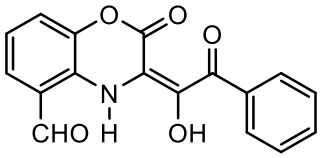
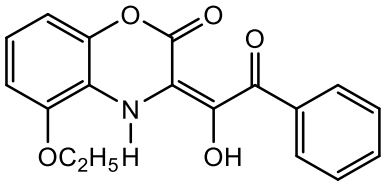
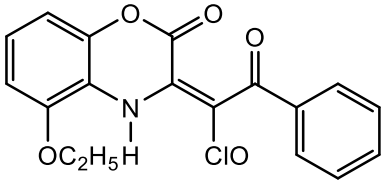
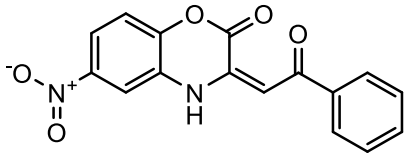
In our way to study the newly designed drug candidates as promising antioxidants compared to ascorbic acid as a reference standard, we performed a molecular docking study for the five new compounds besides the co-crystallised ascorbic acid extracted from the cytochrome c peroxidase enzyme (PDB code: 2X08). The selection of this HEME enzyme as a target for the docking study was based on the fact that it plays a role in neutralising hydrogen peroxide ($HOO^{\cdot}$), thereby contributing to cellular protection against oxidative damage [1]. It was also reported in literature that when this enzyme is dysfunctional, an accumulation of hydrogen peroxide can occur, leading to the production of free radicals. Subsequently, causing significant cellular damage [19]. To validate the docking results, the co-crystallised ligand (ASC) was redocked into the active site. This resulted in a root mean square deviation (RMSD) of 1.3153 Å (Fig. 8), which falls well within the acceptable threshold of ≤2.0 Å, thereby affirming the reliability of the docking approach [12, 24].

The docking results for the designed compound (Table 7) indicate that Compound D5 exhibited the highest binding affinity, with a MolDock score of -135.37 kcal/mol, suggesting strong and stable interactions with the cytochrome c peroxidase receptor. This was followed closely by Compounds D1 and D4, with binding scores of -134.388 and -131.114 kcal/mol, respectively. Compound D3 and D2 recorded moderate MolDock scores of -128.185 kcal/mol and -124.99 kcal/mol. In contrast, the original lead compound (Compound 20) exhibited a comparatively lower binding affinity than designed compounds D5, D1, and D4, with a MolDock score of 128.008 kcal/mol. Remarkably, the design compound exhibited higher binding affinity than the reference

compound with a MolDock score of -82.772 kcal/mol. Furthermore, introduction of the selected functional groups led to a significant enhancement in binding affinity, emphasising their role in optimising ligand-protein interactions and improving potent antioxidant activity.

An analysis of the mechanism of interaction of the designed compounds with the receptor revealed that compound D1 established interaction with the receptor via the formation of two conventional hydrogen bonds with amino residues ARG 48 and LYS 179. Two carbon-hydrogen bonds with the amino residues GLY 178 and ARG 48; a pi-cation interaction with the amino residue ARG 48; a pi-pi stacked interaction with the amino residue TRP 51; two alkyl interactions with the amino residues MET 172 and ALA 174; and eleven pi-alkyl interactions with the amino residues 3ARG 48, HIS 175, 2VAL 47, 2ALA 174, VAL 45, TRP 51, and HIS 175 (Fig. 9a). Compound D2 interacted with the macromolecule via two conventional hydrogen bonds with the amino acid residues HIS 175 and TRP; a carbon-hydrogen bond via MET 172; a sulphur-x interaction with MET 172; two pi-pi stacked interactions with TRP 51; an alkyl interaction with PRO 145; and seven pi-alkyl interactions with HIS 52, ALA 174, TRP 51, 2PRO 145, MET 172, and LEU 171 (Fig. 9b). Compound D3 interacted with the macromolecule via three conventional hydrogen bonds with the amino acid residues ARG 48, HIS 175, and TRP 51; a carbon-hydrogen bond via the amino residue MET 172; a sulphur-x interaction via MET 172; two pi-pi stacked interactions via TRP 51; and five pi-alkyl interactions via the amino residues 2PRO 145, MET 172, LEU 171, and ALA 174 (Fig. 9c). Compound D4 formed two conventional hydrogen bonds with the receptor via amino residues HIS 175 and TRP 51; two carbon-hydrogen bonds via MET 172 and PRO 145; a sulphur-x interaction via MET 172; two pi-pi stacked interactions with TRP 51; one alkyl interaction with PRO 145; and eight pi-alkyl interactions via HIS 52, TRP 51, 2ALA 174, MET 172, 2PRO 145, and LEU 171 (Fig. 9d). Compound D5 formed an interaction with the receptor via two conventional hydrogen bonds with ARG 48 and LYS 179; three carbon-hydrogen bonds with GLYS 178, HIS 175, and ARG 48; a pi-cation interaction with ARG 48; a pi-pi stacked interaction with TRP 51; and nine pi-alkyl interactions (Fig. 9e). Notably, all the designed compounds showed enhanced and diverse interactions compared to the lead compound twenty (20) and most of the active amino acid residues.

Table 7. Chemical structures, predicted pIC_{50} and docking scores of the newly designed compounds.

S/No	Compounds	predicted pIC_{50}	MolDock score	Rerank score
1		8.266	-134.388	-91.39
2		8.534	-124.99	-109.18
3		8.269	-128.185	-112.925
4		8.190	-131.144	-115.329
5		8.004	-135.37	-70.241
Comp 20		7.817	-130.008	-122.325

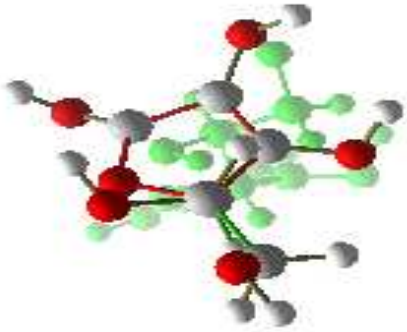


Fig. 8: Superimposition of co-crystallized ligand showing the consistency of the docking algorithm with RMSD value of 1.3153 Å

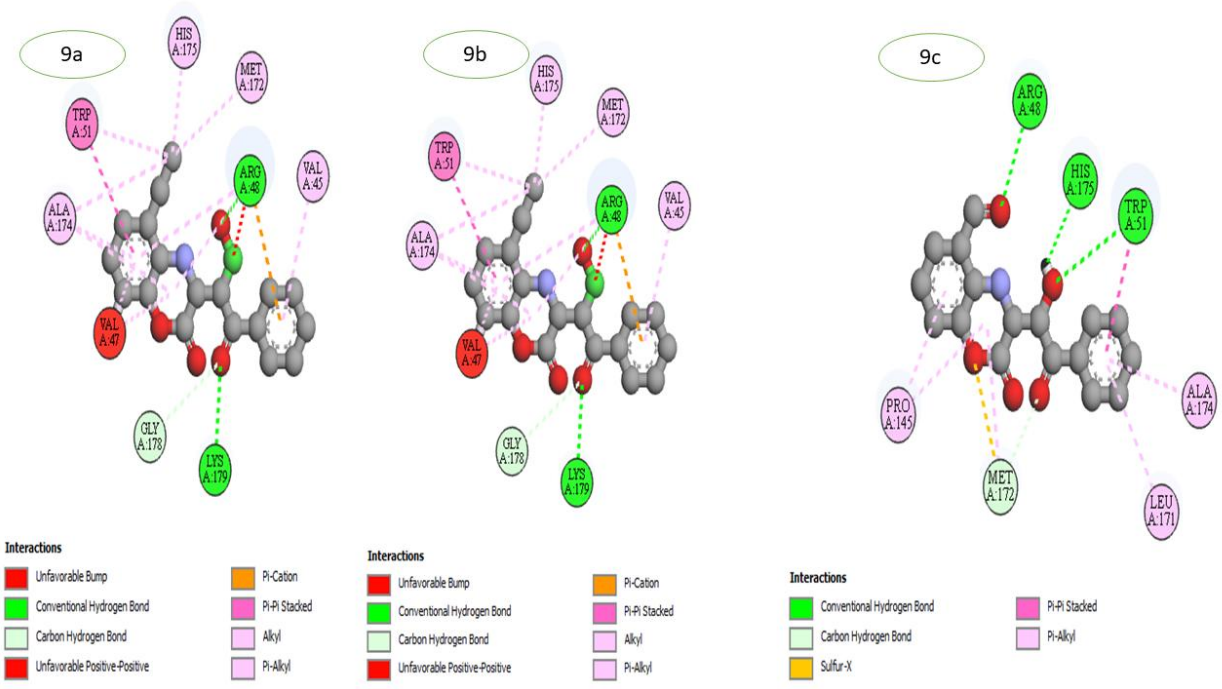


Fig. 9a: 2D Docking view of D1. Fig. 9b: 2D Docking view of D2. Fig. 9c: 2D Docking view of D3

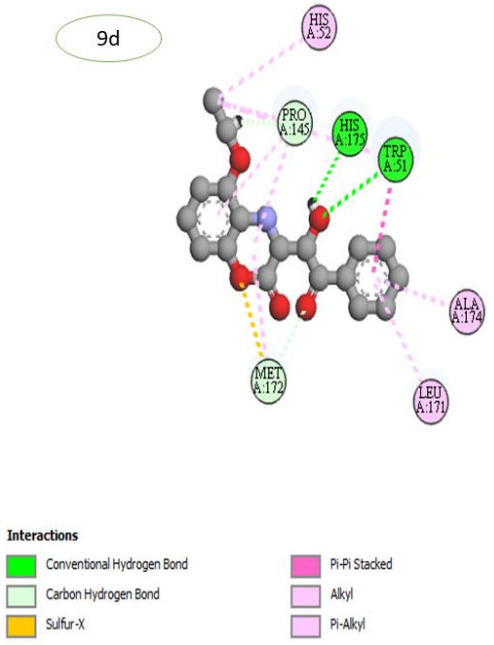


Fig. 9d: 2D Docking view of D4.

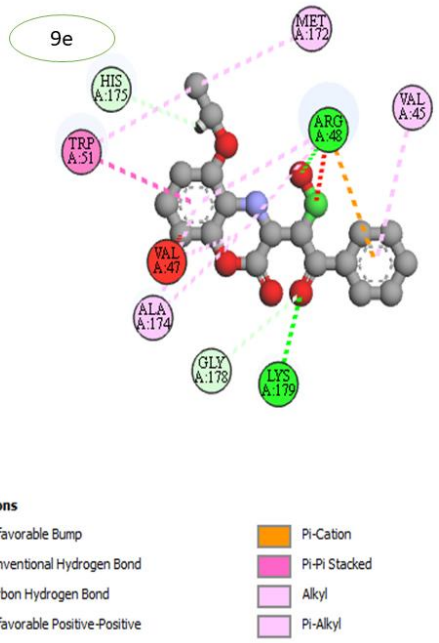


Fig. 9e: 2D Docking view of D5.

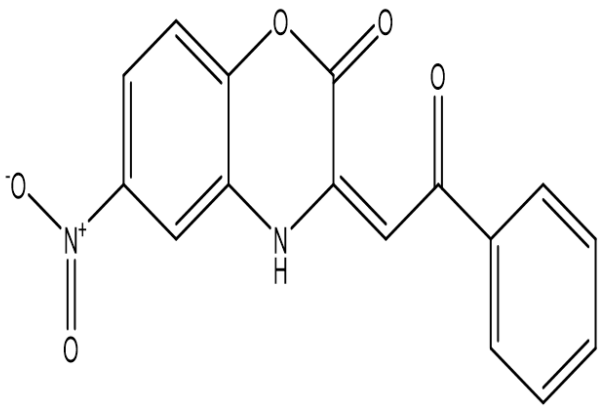


Fig. 10: Structure of compound 21

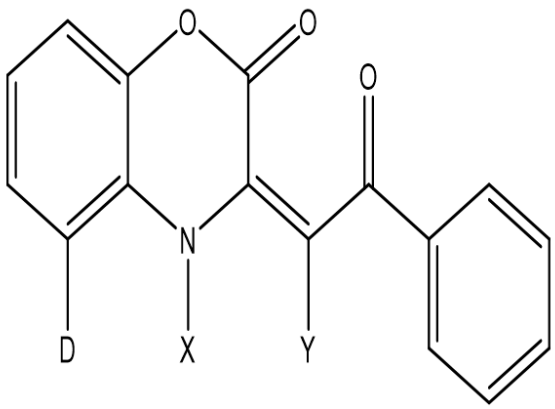


Fig. 11: Structure of the template chosen for design

3.5. The drug-likeness parameters for benzoxazines and the designed compounds.

To take drug development to a higher level with good efficacy, the proper ADMET properties of the drug must be studied at an early stage of the drug discovery process [11]. Moreover, oral absorption of drugs by patients due to its convenience, non-invasiveness, and high patient compliance is a crucial key aspect to be ascertained during the drug discovery process [21]. To achieve this goal, evaluation of drug-likeness, which focuses on measures of oral bioavailability of bioactive compounds, is important in modern drug design. Table 8 depicts the computed drug-likeness properties of the benzoxazines and the designed compounds.

It can be deduced from the outcome results that all the studied compounds display recommendable values based on Lipinski's rule and the Verber rule. Pharmacokinetic properties, such as log P, molecular weight, number of hydrogen bond donors and acceptors, synthetic accessibility, polar surface area, and gastrointestinal absorption values of benzoxazines and designed compounds, fall within permissible limits. This suggests that the compounds do not possess oral bioavailability problems. The studied compounds can be considered for pharmacological applications because they have higher metabolic activity, greater solubility, and excellent oral absorption, as indicated by their lipid affinity values that meet the threshold ($Log \leq 5$) set by Lipinski's rule and Verber's rule [14]. The molecular weight of the benzoxazines and designed compounds falls within the recommended limits ($mw < 500$). Remarkably, molecular weights of designed compounds appeared to be lower compared to the derivatives. This suggests that the new compounds will be easily transported, diffused, and absorbed as compared to heavy molecules [14]. The HBD values of both benzoxazines and designed compounds were observed to be less than five (5), and HBA values were also less than ten (10), demonstrating that they are highly soluble in cell membranes [29]. The TPSA values of both of the studied compounds indicate that they will exhibit sufficient solubility and oral bioavailability because the values were found to be within 63.07-118.12. These values are within the permissible limit (TPSA $\leq$ 140). Computed scores for synthetic accessibility values indicate that all the compounds have S.A. values within the 3.0 range, respectively. This means that even the designed compounds will easily undergo synthesis [12, 14]. All the designed compounds and benzoxazines possess a small number of rotatable bonds (nROTB < 10). Suggesting that the compounds demonstrate excellent flexible interaction with the receptor 2XO8.

Table 8. Drug likeness parameters of the 1,4 benzoxazines derivatives and the designed compounds

S/No	Log P	MW	n-ROTB	n-HBA	n-HBD	S. A	TPSA	GIA	Lipinski's violations
Rule	≤5	< 500	< 10	< 10	≤ 5	<10	≤ 140	-	≤ 1
1	2.52	265.26	2	3	1	3.14	63.07	High	0
2	2.52	295.29	3	4	1	3.14	72.3	High	0
3	3.05	299.71	2	3	1	3.09	63.07	High	0
4	3.37	317.7	2	4	1	3.09	63.07	High	0
5	3.59	334.15	2	3	1	3.1	63.07	High	0
6	4.09	368.6	2	3	1	3.19	63.07	High	0
7	3.68	378.6	2	3	1	3.09	63.07	High	0
8	3.39	313.74	2	3	1	3.18	63.07	High	0
9	3.07	329.73	3	4	1	3.12	72.3	High	0
10	3.15	297.28	2	4	1	3.25	63.07	High	0
11	3.92	348.18	2	3	1	3.31	63.07	High	0
12	2.85	309.32	3	4	1	3.27	72.3	High	0
13	3.49	358.19	2	3	1	3.27	63.07	High	0
14	3.75	376.18	2	4	1	3.25	63.07	High	0
15	4.54	427.08	2	3	1	3.31	63.07	High	0
16	4.07	437.08	2	3	1	3.26	63.07	High	0
17	3.79	372.21	2	3	1	3.35	63.07	High	0
18	2.1	324.29	3	5	1	3.31	108.89	High	0
19	1.92	310.26	3	5	1	3.2	108.89	High	0
20	1.88	310.26	3	5	1	3.26	108.89	High	0
21	2.15	328.25	3	6	1	3.25	108.89	High	0
22	1.69	340.29	4	6	1	3.29	118.12	High	0
23	1.87	310.26	3	5	1	3.26	108.89	High	0
24	2.19	328.25	3	6	1	3.25	108.89	High	0
25	2.4	344.71	3	5	1	3.23	108.89	High	0
26	2.94	379.15	3	5	1	3.31	108.89	High	0

Table 8 continued

S/No	Log P	MW	n-ROTB	n-HBA	n-HBD	S. A	TPSA	GIA	Lipinski's violations
Rule	≤5	< 500	< 10	< 10	≤ 5	<10	≤ 140	-	≤ 1
27	2.49	389.16	3	5	1	3.25	108.89	High	0
28	1.83	340.29	4	6	1	3.28	118.12	High	0
D1	2.95	343.76	4	4	1	3.52	80.14	High	0
D2	2.92	309.32	3	4	2	3.58	83.3	High	0
D3	1.99	309.27	3	5	2	3.42	100.37	High	0
D4	2.54	325.32	4	5	2	3.53	92.53	High	0
D5	3.43	343.76	4	4	1	3.61	72.3	High	0

Key: **MV**: molecular weight**,** $\boldsymbol{Log\ P_{o/w}}$ partition coefficient between octanol and water, **nHBD:** number of hydrogen bond donors, **nHBA:** number of hydrogen bond acceptors, **GIA:** Gastro-intestinal absorption, **TPSA:** Topological polar surface area, **S.A:** Synthetic accessibility, **nRTB:** number of rotatable bonds.

3.6 The Pharmacokinetic and toxicity profiles of the best-docked compounds

Computational predictions of ADMET properties and toxicity parameters of drug candidates are of paramount interest to researchers because they reduce the number of design cycles, speed up the drug discovery process, provide support for animal ethics by reducing the use of animal models, and enhance clinical study success rates [21]. Table 9 represents the pharmacokinetic and toxicity results of the best docked compounds. It can be deduced from the result that all four compounds can be readily absorbed by the human intestine, with absorption rates exceeding 70%. In other words, their absorption rate observed was between $89.5\ and\ 95.40\%$, suggesting that the compound will pass through the mucosal membrane easily following oral administration [30]. Blood-brain barrier (BBB) permeability and CNS permeability prediction results indicated that all the best-docked compounds are poorly permeable across the BBB (log BB < 0.7). Hence, they cannot induce toxicity to the brain through the CNS [30]. The low CNS penetration values (logPS < 1.7) also indicate that the compounds possess desirable properties because they can minimise potential central neurotoxicity [12]. In the examination of the metabolism results, all the four compounds were observed to act as substrates of CYP3A4, indicating they may undergo hepatic metabolism via this major enzyme [12]. Furthermore, all the best docked compounds were observed to be inhibitors of CYP2C19 and CYP2C9 enzymes, except compound 28 which was

found to be a non-inhibitor of CYP2C9. The four compounds were predicted to be non-inhibitors of the CYP2D6 enzyme. This affirms that the compounds will exhibit minimal risk of variability and thereby reduce the likelihood of adverse drug–drug interactions that will lead to toxicity [30]. Compounds 15, 26, and 28 were observed to possess a positive AMES toxicity test, signifying their non-mutagenic nature. Hence, they will not pose any genotoxic effects after oral administration. Conversely, compound 22 showed a negative AMES toxicity test, suggesting that the compound will cause mutagenic effects and can potentially be carcinogenic [30].

Table 9. Predicted ADMET properties of the best docked compounds

S/No	Intestinal absorption % (absorbed)	BBB permeability (log BB)	CNS permeability (log PS)	CYP2D6 Substrate	CYP2C19 inhibitor	CYP3A4 Substrate	CYP2C9 inhibitor	AMES Toxicity
15	89.562	0.131	−1.559	No	Yes	Yes	Yes	No
22	94.341	−0.461	−2.254	No	Yes	Yes	Yes	Yes
26	89.459	−0.57	−1.858	No	Yes	Yes	Yes	No
28	95.401	−0.674	−2.246	No	Yes	Yes	No	No

3.7. Pharmacokinetic and toxicity profiles of best docked compounds

As observed from Table 10, all five designed compounds can be easily absorbed in the human intestine, owing to the facts that the predicted human intestinal absorption (HIA) values, which range from 90.327 to 94.094%, were observed to be high [12]. The predicted values of Log BB for the designed compounds indicate that they cannot be dispersed to the brain because they were less than 0.3. Therefore, they will not pose any toxicity to the brain [30]. The log PS values for the designed compounds (log PS < 1.9) indicate limited CNS distribution, which is a desirable property for compounds targeting excess free radical production that minimises potential central neurotoxicity [12, 31]. Metabolism, which is a crucial aspect of pharmacokinetic study, was assessed using enzyme endpoints. The metabolic results of the five designed compounds revealed that all of them acted as substrates for the CYP3A4 enzyme and as non-inhibitors for the CYP2D6 enzyme. Thus, this indicates successful metabolism of the compounds via CYP3A4 and low risk of variability due to CYP2D6 polymorphism or drug-drug interactions [12]. Fortunately, all the compounds were observed to be inhibitors of CYP2C19 and CYP2C9 enzymes, except D3 and

D4, which were observed to be non-inhibitors of the CYP2C9 enzyme. In addition, the designed compounds D1, D2, and D3 were observed to be non-carcinogenic and non-mutagenic, except for compounds D3 and D4, which were predicted to be mutagenic with respect to the AMES toxicity test data. In all, the favourable drug-likeness parameters, high acceptable intestinal absorption, restricted CNS penetration, and non-predicted toxicity result of the designed compounds D1, D2, and D3 indicate their potential as orally bioavailable antioxidant agents.

Table 10. Predicted ADMET properties of designed compounds.

S/No	Intestinal absorption % (absorbed)	BBB permeability (log BB)	CNS permeability (log PS)	CYP2D6 Substrate	CYP2C19 inhibitor	CYP3A4 Substrate	CYP2C9 inhibitor	AMES Toxicity
D1	90.327	0.202	−1.994	No	Yes	Yes	yes	No
D2	91.054	0.127	−2.03	No	Yes	Yes	yes	No
D3	94.094	−0.148	−2.343	No	Yes	Yes	No	Yes
D4	91.885	−0.148	−2.291	No	Yes	Yes	No	Yes
D5	91.731	−0.525	−2.246	No	Yes	yes	yes	No

3.8 Molecular dynamic simulation result of designed compounds

Evaluation of the dynamic evolution of a system through molecular dynamic simulation is a very important aspect of in silico studies on ligand-protein interactions. This evaluation is a crucial aspect that helps to support the molecular docking studies. Protein ligand complexes are being studied using the root mean square deviation (RMSD) of protein Cα atoms, hydrogen bond analysis, protein root mean square fluctuation (RMSF), and ligand atoms. These evaluations are carried out in order to look at the fluctuating behaviour and reliability of the ligand-protein complex throughout the duration of the simulation.

RMSD is a fundamental parameter in MD simulation studies, which help to provide a quantitative measure of the structural deviations of a molecular system over time. It established the average distance between atoms of superimposed structures, typically with respect to an initial or reference conformation [22]. Molecular dynamic simulation was performed on the designed compounds D1, and D5, having been identified as compounds with the best binding affinities. The protein backbone RMSD trajectories stabilise around 2.2 to 2.6 Å throughout the 100 ns simulation,

suggesting structural stability. The ligand RMSD remains low during the initial peak at 40 ns, but is followed by a sharp displacement at approximately 45 ns and subsequent stabilisation around 6-7 Å, suggesting ligand reorientation into an alternative binding conformation (Fig. 12a). The RMSD analysis of the D4 protein-ligand complex revealed that the protein's RMSD peaked at approximately 0.8 Å to 1.5 Å around 5 to 10 ns, after which it gradually stabilised between 1.8 and 2.1 Å at 100 ns after initial equilibration, suggesting structural stability throughout the 100 ns simulation. The ligand RMSD displayed moderate fluctuations between 0.5 Å and 2.2 Å at around 95 ns. This suggests the ligand conformational adaptability within the binding pocket of the protein without separation (Fig. 12b).

RMSF helps to account for the mean deviation of atomic positions from their average positions throughout the behaviour of molecular dynamic simulations. It also quantifies residue-level flexibility and dynamical properties of the system. A Plot with a high RMSF value (i.e. RMSF > 3.0 Å) is correlated with increased structural flexibility of a complex, while plots with lower RMSF values are related to structural rigidity [12, 31]. In the RMSF analysis, it was observed that both complexes exhibited similar RMSF profiles. Notably, higher fluctuations were recorded in the N-terminal region, while all residues demonstrated fluctuations of less than 3.0 Å. In Fig. 12C, the majority of residue exhibited low RMSF values ranging from 0.4 to 1.2 Å, suggesting that most parts of the protein remain structurally stable during the simulation. From the plot, it can be suggested that a well-maintained protein conformation is achieved. Several localised peaks were observed around the residues 1-15, 55-65, 75-85, 130-145 and 190-210 with RMSF values between 1.5 and 2.3 Å. These regions possess the likelihood of having solvent-exposed terminal regions that exhibit much more mobility. In addition, a pronounced peak was detected around residue 220, with an RMSF value of 3.5 Å, suggesting substantial local flexibility; another high peak was also noticed near residues 275-280, reaching 3.9 Å, which may correspond to a flexible terminal. These types of fluctuations are usually associated with non-structured regions rather than instability of the protein core. In the analysis of the RMSF plot of Fig. 12D, the majority of the residues showed low fluctuation with values ranging from 0.4 to 1.0 Å, indicating that most regions of the protein remain structurally rigid and stable. Moderate fluctuations were observed around specific residue regions, notably around residues 30-40, 55-65, 70-85, 130-145, and 175-190, with RMSF values of 1.2-2.0 Å. These increased fluctuations likely correspond to loop regions, turns that naturally exhibit greater conformational freedom. Additionally, more distinct higher peaks

were observed near residues 215 to 220, reaching approximately 2.3 Å, which suggests a relatively localised region. Another high peak occurred around residues 275-280, with an RMSF value of 1.6 Å; indicating terminal residue mobility. The initial residue domain also displayed a high RMSF value of 3.8 Å; this is commonly due to increased flexibility of the N-terminal end.

3.9 Protein–ligand interactions

Based on molecular docking results which revealed favourable binding affinities, designed compounds D1 and D5 were selected for further analysis to determine their interaction profiles with the target receptor (PDB ID: 2XO8), focusing on their hydrogen bonds, hydrophobic interactions, water bridges, and ionic contacts, as displayed in Fig. 12e and f. Hydrogen bonding plays a major role in ligand binding. Consideration of hydrogen-bonding properties in computational drug design is a very important aspect, owing to their strong influence on drug specificity, metabolisation and adsorption [21]. The designed compound D1 established hydrogen bond interactions with ASP 79, PRO 80, SER 81, ALA 83, LEU 144, PRO 45, ASP 146, LYS 183, ARG 184, GLY 186, ASP 219, ASN 220, and PRO 233. While D4 established hydrogen bonds with ASP 79, GLY 84, ALA 219, and LYS 183.

Regarding hydrophobic interactions, D1 established interactions with many nonpolar residues, including ARG 48, TRP 1, HIS 5, PRO 80, GGLY 84, ASP 146, GLY 186, TRP 233, and LEU 232. While D4 established nonpolar interaction with PRO 80, ALA 83, ALA 147, HIS 181, LEU 182, TRP 187, ALA 218, AND LEU 232. Water bridge interactions, which often contribute to the stabilisation of ligand–receptor complexes, were also observed. D1 established numerous water-mediated interactions with PRO 80, SER 81, ALA 83, GLY 84, ASP 146, LYS 183, ARG 184, SER 185, GLYS 186, TYR 187, ASN 216, ASN 219, ASN 220, GLU 221, and THR 234, while D4 established water bridge interactions via the residues LYS 74, PHE 77, PRO 80, ASN 87, LEU 182, LYS 183, ARG 184, SER 185, GLYS 186, and TYR 187. Notably, neither of the two designed compounds displays ionic contacts during their binding with the protein's active site residues.

To determine the time-dependent stability of the observed interactions, protein–ligand contact frequencies across the simulation trajectory were quantitatively evaluated and visualised in Fig. 12g and c. The contact counts for the two complexes fluctuated between 0 and 6, indicating dynamic but sustained binding throughout the 100 ns simulation. Moreover, the contact maps

revealed multiple deep and continuous interaction bands, suggesting robust and stable associations between each ligand and a range of amino acid residues.

3.10. Ligand properties analysis

The structural and dynamic behaviours of the designed compounds D1 and D4 were evaluated by determining various key properties, such as compound root mean square deviation (RMSD), radius of gyration (rGyr), polar surface area (PSA), molecular surface area (MolSA), and solvent-accessible surface area (SASA). The results are displayed in Fig. 13a and b. For the designed compound 1 and 4 complexes, the compound RMSD values showed initial fluctuations during the first 10 ns, after which they gradually stabilised. The RMSD value for the designed D1_2XO8 begins at a peak of approximately 0.6 Å, and then reaches an equilibrium value at 0.9 Å. While for D4_2XO8, the RMSD value begins at approximately at 0.4 Å, and then reaching equilibrium value at 0.9 Å. The radius of gyration (rGyr), which account for the compactness of a ligand's structure, also established minimal fluctuations before stabilising. The rGyr values spanned from 3.70 to 3.80 Å for D1_2XO8 (equilibrating at 3.90Å) and 3.75– 3.95 Å for D4_2XO8 with final equilibrium at 4.0 Å. The intramolecular hydrogen Bonds (intra HB), which account for the number of internal hydrogen bonds (HB) within a ligand molecule for D1_2XO8, remain relatively stable (0-1), while intra HB was not detected in D4_2XO8.

Molecular surface area values remained relatively stable, reflecting minor changes in the overall molecular surface. Specifically, MolSA values ranged from 302 to 304 $Å^2$, stabilising at 308 Å2 for D1_2XO8 and 300–304 $Å^2$, and approximately stabilising around 308 $Å^2$ for D4_2XO8 (Fig. 13A and B). Furthermore, the surface area of a molecule accessible by a water molecule (SASA) determination displayed initial variability followed by stabilisation, suggesting steady solvent exposure over time. SASA values for D1_2XO8 ranged from 80 to 240 $Å^2$, and equilibrating at 320 $Å^2$. While D4_2XO8, the values ranged from 240 to 320 $Å^2$, and equilibrating at 390 $Å^2$. Lastly, the polar surface area (PSA), which accounts for the prospect of hydrogen bonding and solubility, stabilises across all complexes after initial adjustments. PSA values ranged between 110 and 125 $Å^2$, and stabilising at 135 $Å^2$ for D1_2XO8. While the PSA values for D4_2XO8 ranged between 138 and 144 $Å^2$, stabilising at approximately 150. Thus, the designed compounds' property assessment across the simulation established mild fluctuations during the early stages,

followed by attaining consistent equilibrium, suggesting that each compound remained stably bound within the protein's active site throughout the 100 ns simulation.

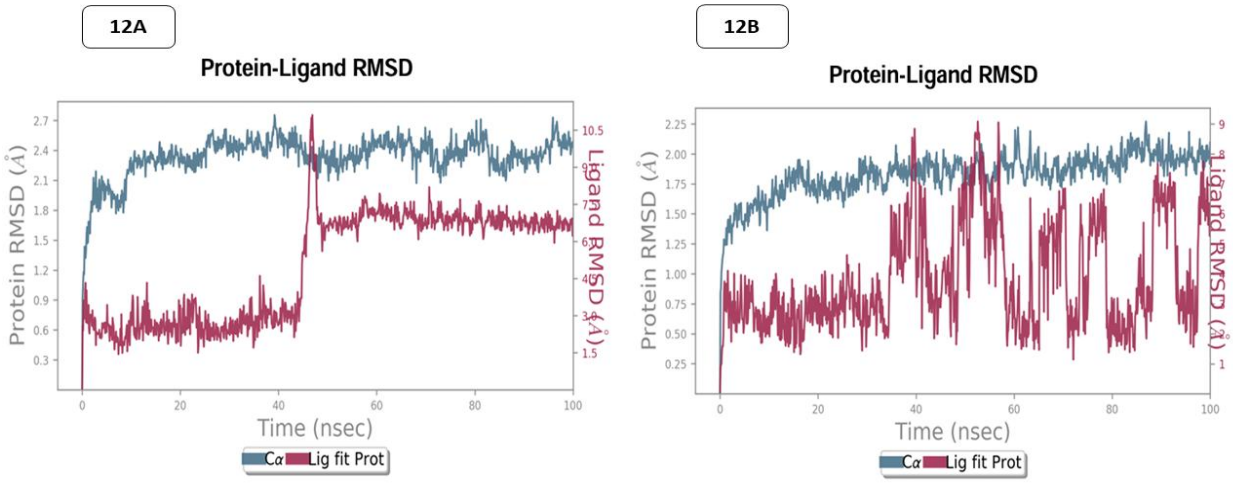


Fig. 12: Comparative RMSD plots of designed complexes (12A) D1_2XO8 (12A) D4_2XO8

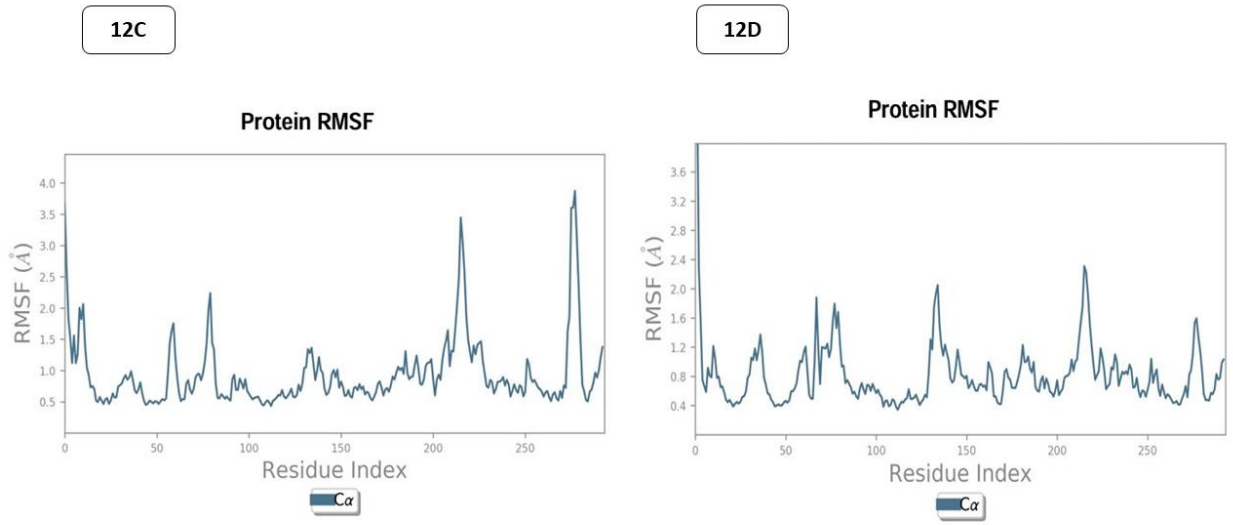
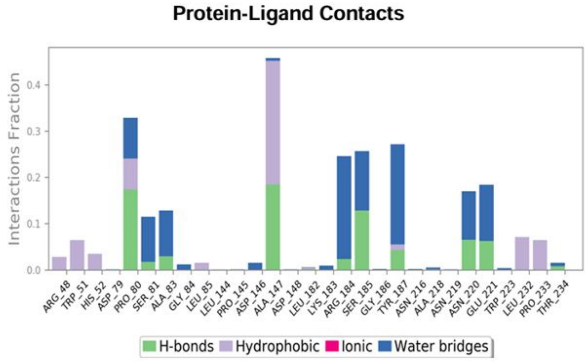


Fig. 12: Comparative RMSF plots of designed complexes (12C) D1_2XO8 (12D) D4_2XO8

12E



12F

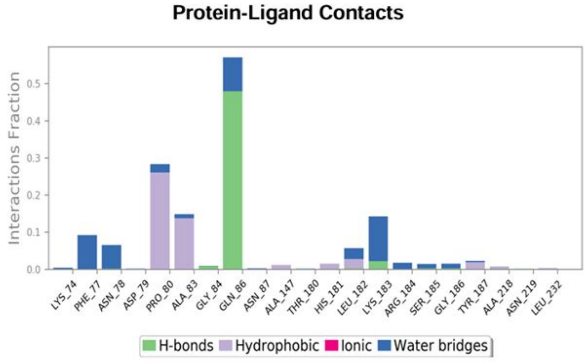
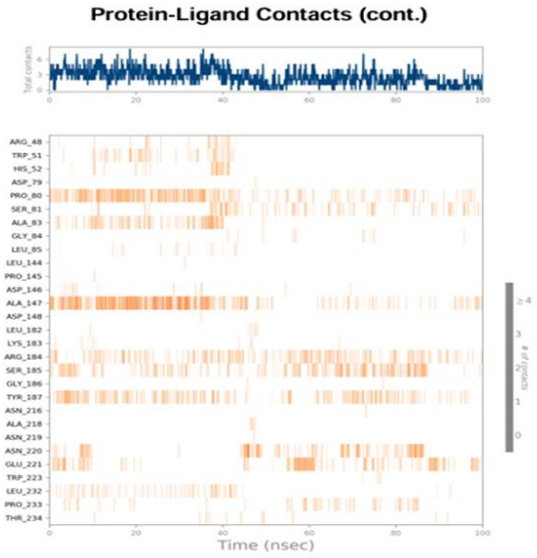


Fig. 12G: Protein-Ligand contacts of D1

Fig. 12G: protein-Ligand contacts of D1

12G



12H

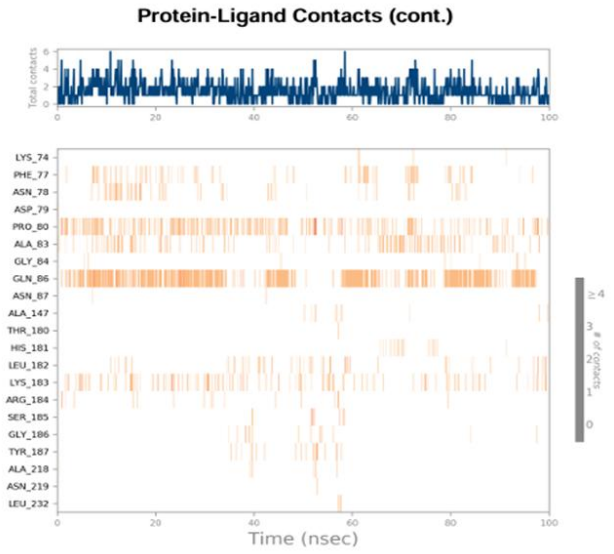


Fig. 12G: Protein-Ligand contacts of D1

Fig. 12G: protein-Ligand contacts of D4

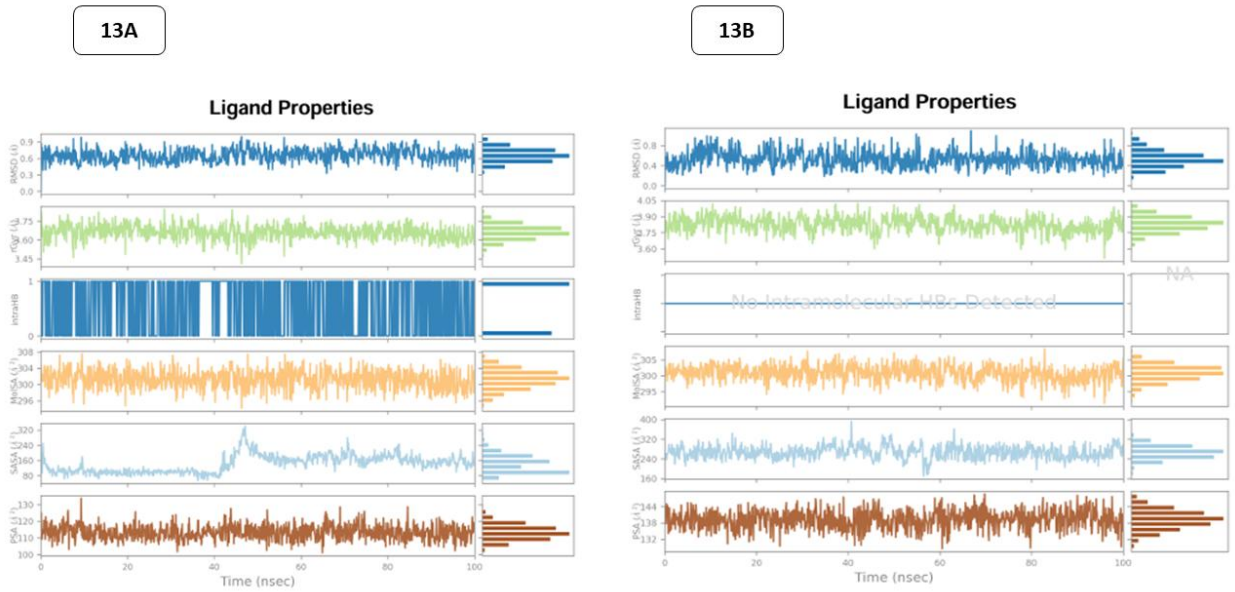


Fig. 13: MD results of ligand property of complexes (13A) D1_2XO8 (13B) D4_2XO8

Conclusion

A data set of twenty-eight bioactive benzoxazine derivatives was used to build a robust, stable, and highly predictive QSAR model linking the in vitro antioxidant properties of the compounds against the DPPH assay to their molecular descriptors. The validated model was used to design a more potent benzoxazine scaffold. The designed compounds were observed to exhibit better biological activities than the selected template structure and Vitamin C standard. Furthermore, significant correlation was observed between ΔG values obtained for each complex. Additionally, the ligands were observed to possess high pharmacokinetic profiles. Thus, the study suggests potential advantages of the new benzoxazine-based inhibitors of excess free radical production as potential therapeutic agents against oxidative stress, subject to further in vitro and in vivo investigations.

Funding

This research work received no external funding.

Declaration of Competing Interest

The authors declared that they have no known competing financial interests or personal relationships that could have appeared to influence the work reported in this paper.

CRediT authorship contribution statement

Muhammad Baba Muhammad: Conceptualization, Data curation, Visualization, Writing – original draft. Adamu Uzairu: Methodology, Investigation, Supervision. S.E Abechi: Software, Visualization, Validation, Writing – review & editing, Muhammad Tukur Ibrahim: Supervision, Software, Visualization, Validation, Writing – review and editing.

Acknowledgement

The authors expressed their profound gratitude to G.F.S. Harrison Quantum Chemistry Research Group in the Department of Chemistry, Ahmadu Bello University, Zaria for technical support and encouragement.

Clinical trial number

Not applicable.

Ethics

Not applicable

Consent to participate

Not applicable

Consent to publish declaration

Not applicable

Ethics declaration: Not applicable

Data availability declaration

The author declared that the raw data that support the findings of this study are available in the Edinburgh DataShare repository with the identifier below:

https://doi.org/10.3389/fchem.2018.00056

References.

[1]. M.M Ismail Othman, A.M. Mohamed, E. Gad-Elkareem, A. Kaiss, A. Mejdi, S. Adel Kadri. New substituted pyrazalones and dipyrazolotriazines as promising tyrosyl-Trna synthetase and peroxiredoxin-5 inhibitors: Design, synthesis, molecular docking and structure-activity relationship (SAR) analysis, J. Bioorganic chemistry (2021) 104704, doi.org/10.1016/j. bioorg.2021.104704.

[2]. A.Z. Maged, S.S. Wesam, A.A. Ahmed, H.A. Magda, Design, synthesis, biological evaluation, 2D QSAR Modeling, and molecular docking studies of novel 1H-3-Indolyl derivatives as significant antioxidants, Int. J. Mol. Sci. 22 (2021) 10396, doi:10.3390/ijms221910396.

[3]. N. Farah, E. Fatemeh, the response of glutathione oxidase and cytochrome c to exercise training and sodium selenite in the heart tissue of male rats, Biochemistry and Biophysics Reports 44 (2025) 102337, doi.org/10.1016/j.bbrep.2025.102337.

[4]. S. Jeremic', S. Radenkovic', S. Filipovic´, M. Antic´, M.A. Amic´, A., Z. Markovic Importance of hydrogen bonding and aromaticity indices in QSAR modeling of the antioxidative capacity of selected (poly)phenolic antioxidants, J. Mol. Graph Model 72 (2017) 240–245, doi:10.1016/j. jmgm.2017.01.011.

[5]. B.R. Bashir, B.U. Abdullahi, Investigating the potential of novel antioxidant flavonoids: a comprehensive study of drug-likeness, molecular docking, pharmacokinetics, and DFT analysis, Future J. Pharm. Sci. 11 (18) (2025) 2–17, doi:10.1186/s43094-025-00837-z.

[6]. S.F. Norma, S.C. Raúl, V.C. Claudia, H.C. Beatriz, Antioxidant compounds and their antioxidant Mechanism, Intechopen, doi.org/10.5772/intechopen.85270.

[7]. S. Vashundhra, J.K. Pradeep, S. Mukesh, Y.K. Dharmendra, M.M. Saloni, S.K. Ajit, M. Sanjeev, K. Mi-hyun, C. Sandeep, Discovery of C-3 Tethered 2-oxo-benzo [1,4] oxazines as potent antioxidants: Bio-inspired based design, synthesis, biological evaluation, cytotoxic, and in silico molecular docking studies, frontiers in chemistry, doi: 10.3389/fchem.2018.00056.

[8]. A. Shahin, M Mehrshad, R. Sahar, M. Noushin, Structure-activity relationship of the radical scavenging activities of some natural antioxidants based on the graph of atomic orbitals, Journal of Molecular Structure, (2019) 165-74, doi.org/10.1016/j.molstruc.2019.04.103

[9]. F. Theano, P. Adamantia, T. Andromachi, M. Michail, P. Harris, K. Maria, K. Dimitris, M. Eleni, C. Theodora, Design and synthesis of novel antioxidant benzoxazine hybrids and their effects on Fibroblasts, Antioxid. MDPI 13 (2024) 798, doi.org/10.3390/antiox 13070798.

[10]. H.B. Manel, A. Iqrar, H. Assi, D. Amal, P. Harun, B. Nouha, H.S. Walid, H. Sabri, H. Karim, G. Siwar, A. Fahad, N. Emira, S. Mejdi, A. Kaïss, K. Adel, Design, synthesis, biological evaluation and in silico studies of novel 1,2,3-triazole linked benzoxazine 2,4-dione conjugates as potent antimicrobial, antioxidant and anti-inflammatory agents, Arabian Journal of Chemistry (2022) 15, doi.org/10.1016/j.arabjc.2022.104226.

[11]. A. Nourah, A. Emilia, Synthesis and antimicrobial, Applications of 1,3-Benzoxazine derivatives: A Review, Malaysian Journal of Chemistry, (2025) 27(2), 33-53.

[12]. A.B. Sagiru, A. Hamza, A. Uzairu, G.A. Shallangwa, S. Uba, A.B. Umar, Ligand-based drug design of quinazolin-4(3H)-ones as breast cancer inhibitors using QSAR modeling, molecular docking, and pharmacological profiling, Journal of the Egyptian National Cancer Institute. doi.org/10.1186/s43046-023-00182-3.

[13]. M. Abdullahi, A. Uzairua, G.A. Shallangwa, P.A. Mamza, M.T. Ibrahim, Computational modelling of some phenolic diterpenoid compounds as anti-influenza A virus agents, Sci. Afr. 19 (2023) e01462, doi: 10.1016/j.sciaf.2022. e01462.

[14]. S.C. Ja'afaru, A. Uzairu, R.A. Costa, M.S. Sallau, M.T. Ibrahim, Ligand-based virtual screening and QSAR modelling for the discovery of potent SmHDAC8 inhibitors, Silico Res. Biomed. 1 (2025) 100044, doi:10.1016/j. insi.2025.100044.

[15]. A. Moulishankar, T. Sundarrajan, QSAR modeling, molecular docking, dynamic simulation and ADMET study of novel tetrahydronaphthalene derivatives as potent antitubercular agents, Beni-Suef Univ. J. Basic Appl. Sci. 12 (2023) 1–20, doi:10.1186/s43088-023-00451-z.

[16]. D. Ossama, E. Souad, C. Samir, E. Rachida, Z. Hsaine, B. Touimi, QSAR, molecular docking and ADMET studies tetrahydrobenzothiazole derivatives as potential anti-tumor agents, Heliyon 7 (2021) e07463D. Ossama, E. Souad, C. Samir, E. Rachida, Z. Hsaine, B. Touimi, QSAR, molecular docking and ADMET studies tetrahydrobenzothiazole derivatives as potential anti-tumor agents, doi: 10.1016/j. heliyon.2021e074763.

[17]. S.A. Khalifa, A. Uzairu, E.A. Stephen, G.A. Shallangwa, B.U. Abdullahi, A search for novel antidiabetic agents using ligand-based drug design and molecular docking studies employing human intestinal maltase-glucoamylase as model enzyme, Adv. J. Chem. 6 (2) (2023) 155–171, doi:10.22034/ajca.2023.387041.1355.

[18]. S. Prateek, T. Aman, G. Anju, G.S. Ajmer, Molecular docking, 2D-QSAR and ADMET studies of 4-sulfonyl-2-pyridone heterocycle as a potential glucokinase activator, Results in Chemistry 6 (2023) doi.org/10.1016/j.rechem.2023.101105.

[19]. M. Paolo, D. Simona, S. Anna, S. Mariarosaria, The Cu, Zn Superoxide Dismutase: Not Only a Dismutase Enzyme. Front Physiol. 7 (2016) 594, doi:10.3389/fphys.2016.00594.

[20]. K. Misra, T. Anushree, Molecular docking, A structure-based drug design approach, JSM Chem. 5 (2) (2017) 1042 doi:10.47739/2334-1831/042.

[21]. B. Hayet, K. Belbah, Z. Belguidoum, F. Ourdjini, H. Zahra, M. Fatiha, N. Leila, N. Mouna, H. MohammedHad, B. Mortada, G.A. Habiba, C. Abdelkader, Enhancing the antioxidant potential of a coumarin derivative via nickel complexation: synthesis, spectral insights, DFT analysis, and molecular docking, *RSC Adv* (2025) 15, 30102. doi:10.1039/d5ra03168k

[22]. S. Supriyo, S. Prinsa, M.A. Sarkar, Natural flavonoids as primary amoebic Meningoencephalitis Inhibitor: virtual screening and molecular docking studies. *Chem Biodivers.* 22 (2025) e202402521, doi:10.1002/cbdv.202402521.

[23]. J.A. Philip, A. Uzairua, G.A. Shallangwa, S. Uba, M.T. Ibrahim, In-silico design of some tetrazoloquinoline analogs as potent inhibitors of DNA gyrase of Salmonella typhi: QSAR modeling, molecular docking, MD simulation, and ADMET profiling, Silico Res Biomed. 1 (2025) 100121, doi:10.1016/j. insi.2025.100121.

[24]. B.S. Abubakar, A. Uzairu, G.A. Shallangwa, I. Abdulkadir, A.A. Razzak Mahmood, M.T. Ibrahim, Molecular dynamics simulation, Molecular docking, ADMET prediction, QSAR modeling and density functional theory computation for the identification of possible Hepatitis C Virus NS5B Protease inhibitors through in silico study of fluorine-2, 7-diamine compounds, In silico Res. Biomed. 1 (2025) 100104, doi.org/10.1016/j.insi.2025.100104.

[25]. T.A. Nyijime, A.B. Umar, G.A. Shallangwa, M.T. Ibrahim, A. Uzairu, A.C. handra, S. Nagendra, Computational design and evaluation of anilinoquinazoline derivatives as potential anti-tuberculosis agents: DFT, docking, ADMET, and molecular dynamics simulation, The Microbe 10 (2026) 100683 doi.org/10.1016/j.microb.2026.100683.

[26]. A.N. Thomas, G.A Shallangwa, A. Uzairua, A.B. Umar, M.T. Ibrahim, A. Mohad, H. Abdullah, B. Jameel, M.A Hassan, In Silico design and evaluation of novel anti tubercular agents as Inha inhibitors through a virtual screening approach, Discover Chemistry. (2025) 2, 299 doi.org/10.1007/s44371-025-00367-w.

[27]. E. Setiawan, M. Mudasir, Quantitative structure–activity relationship study to predict the antibacterial activity of gemini quaternary ammonium surfactants against Escherichia coli, J. of Applied Pharmaceutical Science, 7 (2022) 12, 099-105, doi:10.7324/JAPS.120710

[28]. Y. Mithlesh, N.M. Suraj, S. Bharti, Y. Haya, P. Rohit, S.P. Gurubasavaraja, Archana K. Synthesis, antioxidant, antimicrobial activities and molecular modeling analysis of some 5-Nitro-N-phenyl-3 (phenylamino)-1H-indazole-1-carboxamide derivatives, Chem. Phys. Impact 9 (2024) 100705, doi:10.1016/j. chphi.2024.100705.

[29]. A.U. Bello, A. Uzairu, Molecular modeling strategy to design novel anticancer agents against UACC-62 and UACC-257 melanoma cell lines, Egyptian journal of basic and applied sciences, (2023) 10 (1), 157–173, doi.org/10.1080/2314808X.2022.2161037.

[30]. K.N. Avika, Y. Haya, S. Shikha, M.N. Suraj, G. S. Shailesh, Studies on chlorophenyl, thiophenyl, and biphenyl clubbed tetrahydro bipyrazole carbaldehydes: Synthesis, antimicrobial and antioxidant activity, SAR study, in-silico pharmacokinetics, toxicity, and molecular modeling, Chemical Physics Impact 9 (2024) 100713. doi.org/10.1016/j.chphi.2024.100713.

[31]. E.I. Emmanuel, A. Uzairu, M.A. Paul, G.A. Shallangwa, M.T. Ibrahim, Design of some potent non-toxic Autoimmune disorder inhibitors based on 2D-QSAR, CoMFA, molecular docking, and molecular dynamics investigations, Intelligent Pharmacy, (2023) doi.org/10.1016/j.ipha.2023.12.009.

[32]. M. Abdul-Hammed, I.O. Adedotun, M. Olajide, C.O. Irabor, T.I. Afolabi, I.O. Gbadebo, L. Rhyman, P. Ramasami, Virtual screening, ADMET profiling, PASS prediction, and bioactivity studies of potential inhibitory roles of alkaloids, phytosterols, and flavonoids against COVID-19 main protease, Nat. Prod. Res. (2021) 1–7, doi:10.1080/14786419. 2021.1935933.